

# Supplementary Information

## **Real-time visualisation of fast nanoscale processes during liquid reagent mixing by liquid cell transmission electron microscopy**

*Govind Ummethala<sup>1,2</sup>, Ravi Jada<sup>3</sup>, Shourya Dutta-Gupta<sup>1</sup>, Junbeom Park<sup>4</sup>, Amir H Tavab<sup>2</sup>, Shibabrata Basak<sup>4</sup>, Robert Hooley<sup>5</sup>, Hongyu Sun<sup>6</sup>, H Hugo Pérez Garza<sup>6</sup>, Rüdiger-A Eichel<sup>4</sup>, Rafal E Dunin-Borkowski<sup>\*\*2</sup>, Sai Rama Krishna Malladi<sup>\*1</sup>*

---

<sup>1</sup> Department of Materials Science and Metallurgical Engineering, Indian Institute of Technology Hyderabad, Kandi, Sangareddy 502285, Telangana, India

<sup>2</sup> Ernst Ruska-Centre for Microscopy and Spectroscopy with Electrons and Peter Grünberg Institute, Forschungszentrum Jülich GmbH, 52425 Jülich, Germany

<sup>3</sup> Advanced Organic Photonic Materials and Technology Laboratory, School of Chemistry and Centre for Nanotechnology, University of Hyderabad, Gachibowli, Hyderabad 500046, India

<sup>4</sup> Institute of Energy and Climate Research, Fundamental Electrochemistry (IEK-9), Forschungszentrum Jülich GmbH, 52425 Jülich, Germany

<sup>5</sup> TESCAN Brno s.r.o, Brno, South Moravia, Czechia

<sup>6</sup> DENSSolutions B.V., Delft, The Netherlands

# Contents

<b>1</b>	<b>Material Synthesis, Self-Assembly, and <i>Ex Situ</i> Characterisation</b>	<b>3</b>
1.1	Chemicals	3
1.2	Material Synthesis	3
1.2.1	Nuclear Magnetic Resonance (NMR)	5
1.3	Self-Assembly	8
1.4	<i>Ex Situ</i> Characterisation	9
1.4.1	X-Ray Diffraction (XRD)	9
1.4.2	Field Emission Scanning Electron Microscopy (FESEM)	10
1.4.3	Influence of Substrate on Particle Growth	11
1.4.4	Transmission Electron Microscopy (TEM)	14
1.4.5	Low-dose 4D-STEM	16
<b>2</b>	<b>Methods</b>	<b>19</b>
2.1	Holder Design	19
2.2	Nano-Cell Design & Chip Assembly	20
2.3	Liquid Flow	22
<b>3</b>	<b>Electron dose</b>	<b>24</b>
<b>4</b>	<b><i>In Situ</i> Liquid Cell Trials</b>	<b>26</b>
4.1	Graphene Liquid Cells (GLCs)	26
4.2	DENSolutions Ocean Holder	27
4.3	DENSolutions Steam Holder	29
<b>5</b>	<b>Data Analysis</b>	<b>30</b>
5.1	Determining Growth Rate of Particles - Experiments without Methanol	30
5.2	Statistical Analysis and Growth Rate of Particles - Antisolvent Crystallisation	32
<b>6</b>	<b>Supplementary Tables</b>	<b>36</b>
<b>7</b>	<b>List of Movies and Captions</b>	<b>37</b>
<b>8</b>	<b>Supplementary References</b>	<b>39</b>

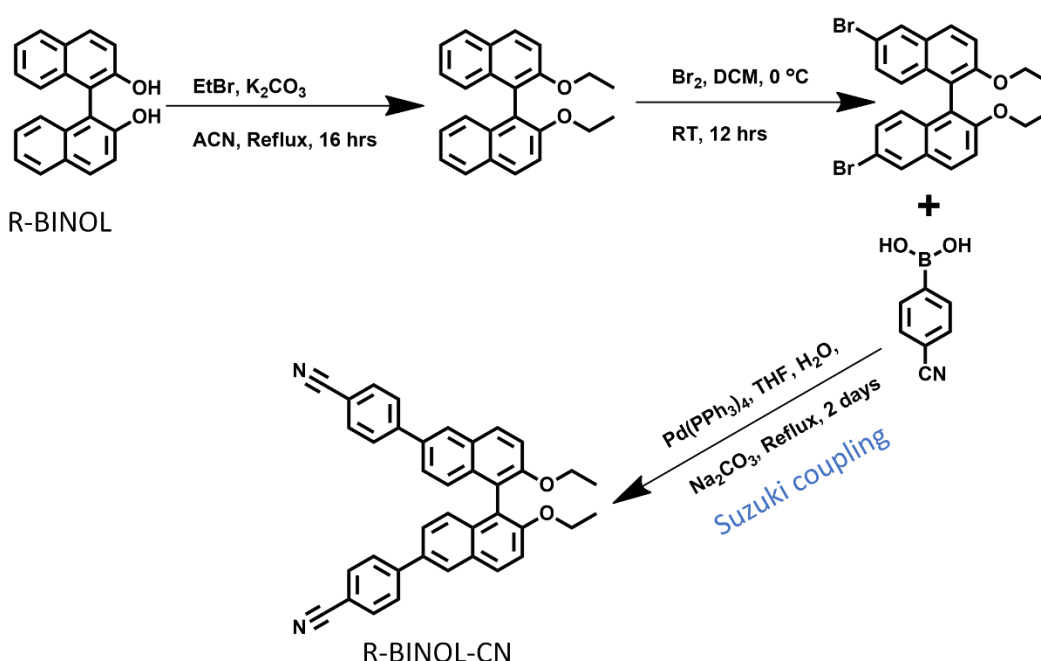
# Supplementary Note 1

## 1 Material Synthesis, Self-Assembly, and *Ex Situ* Characterisation

### 1.1 Chemicals

4-cyanophenylboronic acid ( $\geq 95\%$ ),  $\text{CDCl}_3$  (99.8%),  $\text{Pd}(\text{PPh}_3)_4$  (99%), Bromine ( $\geq 99.5\%$ ), Ethyl bromide ( $\geq 98.5\%$ ), Acetonitrile, Dichloromethane, Tetrahydrofuran and Ethyl acetate and HPLC grade solvents were purchased from Sigma-Aldrich chemicals.  $\text{K}_2\text{CO}_3$ ,  $\text{Na}_2\text{SO}_4$ ,  $\text{Na}_2\text{CO}_3$  and Sodium bisulfite were obtained from Finar Chemicals Limited. HPLC grade solvents were used for the self-assembly process.

### 1.2 Material Synthesis



Supplementary Fig. 1: Schematic of the R-BINOL-CN synthesis process.

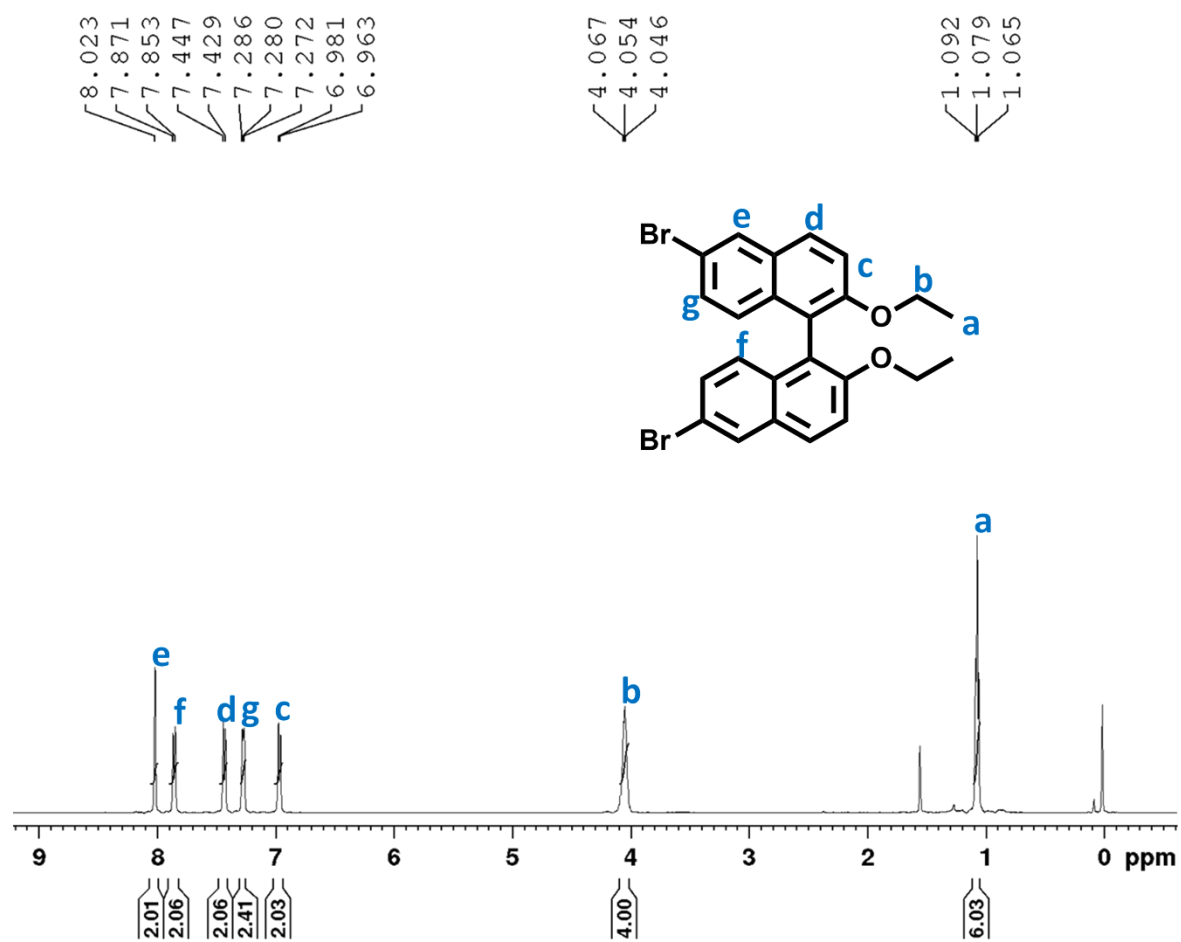
**Synthesis of 2,2'-diethoxy-1,1'-binaphthalene:** The compound 2,2'-diethoxy-1,1'-binaphthalene was synthesized following the procedure reported in the literature<sup>58</sup>. In a clean, dried 100 mL round-bottom flask, ethyl bromide (4 mL, 6 equiv), R-BINOL (2 g, 1 equiv),  $\text{K}_2\text{CO}_3$  (5.8 g, 6 equiv), and acetonitrile (30 mL) were added. The flask was equipped with a water-cooled condenser, and the reaction mixture was heated to reflux for 16 hours. After cooling to room temperature (RT), the reaction was diluted with water and extracted with DCM. The organic layers were dried over  $\text{Na}_2\text{SO}_4$ , concentrated under reduced pressure, and purified by silica gel column chromatography to afford the product as a white solid (1.91 g, 80%).

**Synthesis of 6,6'-dibromo-2,2'-diethoxy-1,1'-binaphthalene:** In a clean and dried 250 mL RB flask, 2,2'-diethoxy-1,1'-binaphthalene (10.0 g, 29.2 mmol, 1 eq.) was dissolved in 100 mL of DCM. The

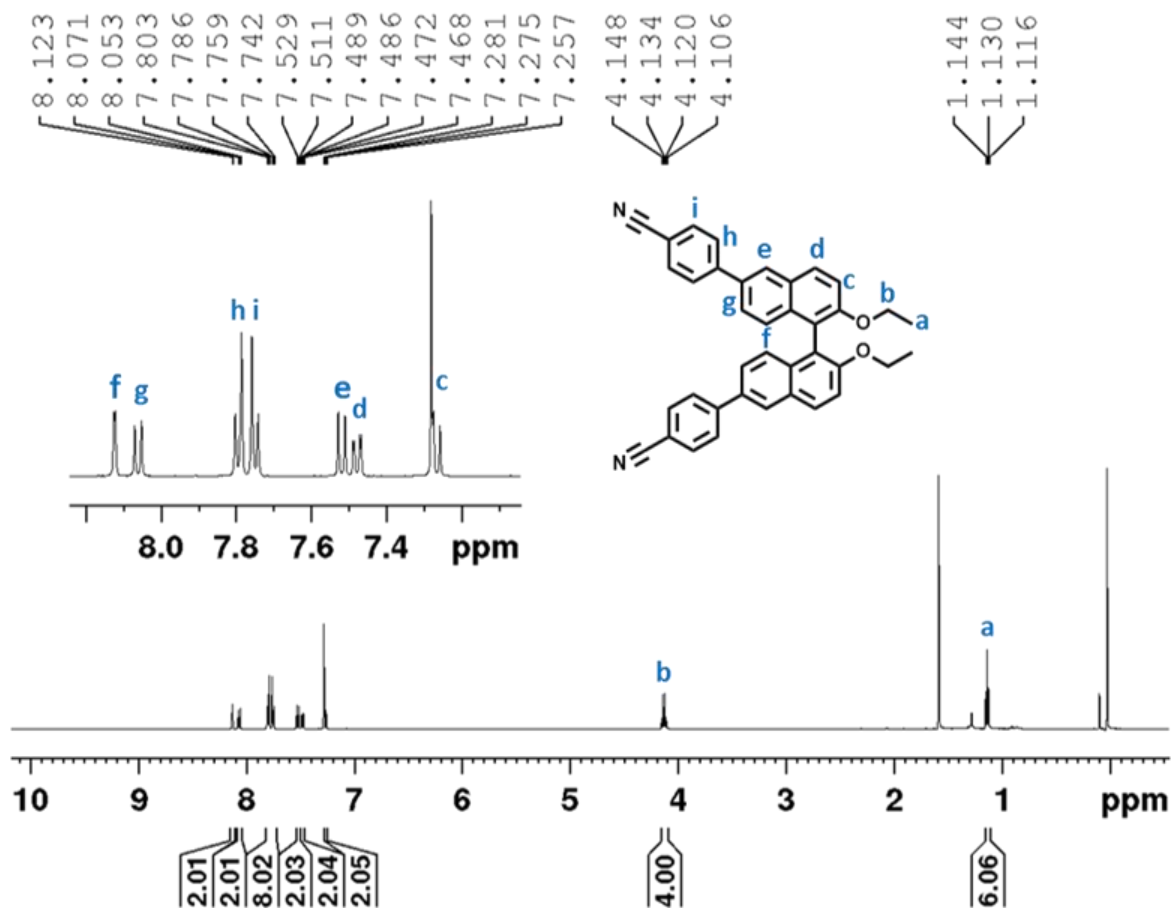
solution was cooled to 0°C and Br<sub>2</sub> (3.16 mL, 61.3 mmol, 2.1 eq.) was added dropwise to the solution under inert conditions. The solution mixture was stirred for 12 hours as it warmed to room temperature. The mixture was quenched with NaHSO<sub>3</sub>, extracted with DCM, and concentrated in a vacuum evaporator. The solid was recrystallised which yielded a white powder (yield, 80%). <sup>1</sup>H NMR (400 MHz, CDCl<sub>3</sub>) δ 8.02 (d, 2H), 7.87 (d, 2H), 7.44 (d, 2H), 7.28 (dd, 2.1 Hz, 2H), 6.98 (d, 2H), 4.05 (4H), 1.07 (t, 6H).

**Synthesis of R-BINOL-CN:** The mixture of 6,6'-dibromo-2,2'-diethoxy-1,1'-binaphthalene (0.309 g, 1 eq.), 4-cyanophenylboronic acid (0.2 g, 2.2 eq.), [Pd (PPh<sub>3</sub>)<sub>4</sub>] (0.107 g, 0.15 eq.), dry THF solvent and aqueous Na<sub>2</sub>CO<sub>3</sub> (0.512 g, 6 eq.) was refluxed under N<sub>2</sub> condition for 2 days. The resultant reaction mixture was extracted with ethyl acetate and the organic layer was dried with Na<sub>2</sub>SO<sub>4</sub>. The solvent was removed, and the colourless solid purified by column chromatography, resulting in a 76% R-BINOL-CN yield. <sup>1</sup>H NMR (400 MHz, CDCl<sub>3</sub>) δ 8.12 (d, 2H), 8.05 (d, 2H), 7.80-7.74 (m, 8H), 7.52 (d, 2H), 7.47 (d, 2H), 7.25 (d, 2H), 4.05 (q, 4H), 1.07 (t, 6H); <sup>13</sup>C NMR (100 MHz, CDCl<sub>3</sub>) δ 155.13, 145.66, 133.98, 133.96, 132.62, 129.91, 129.21, 127.63, 126.38, 125.13, 120.05, 119.03, 116.31, 110.56, 65.10, 29.69, 14.96, 1.01.

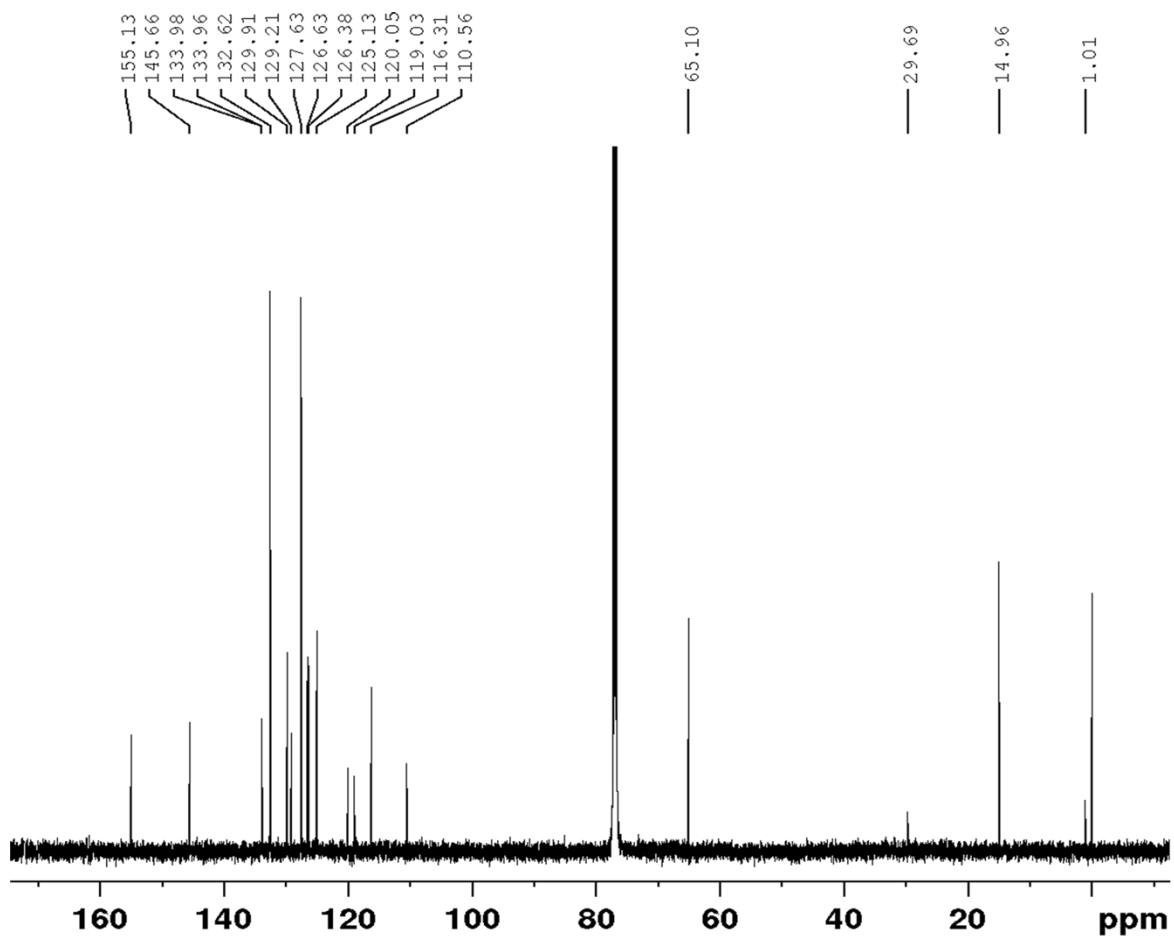
## 1.2.1 Nuclear Magnetic Resonance (NMR)



Supplementary Fig. 2: <sup>1</sup>H-NMR spectrum of 6,6'-dibromo-2,2'-diethoxy-1,1'-binaphthalene.

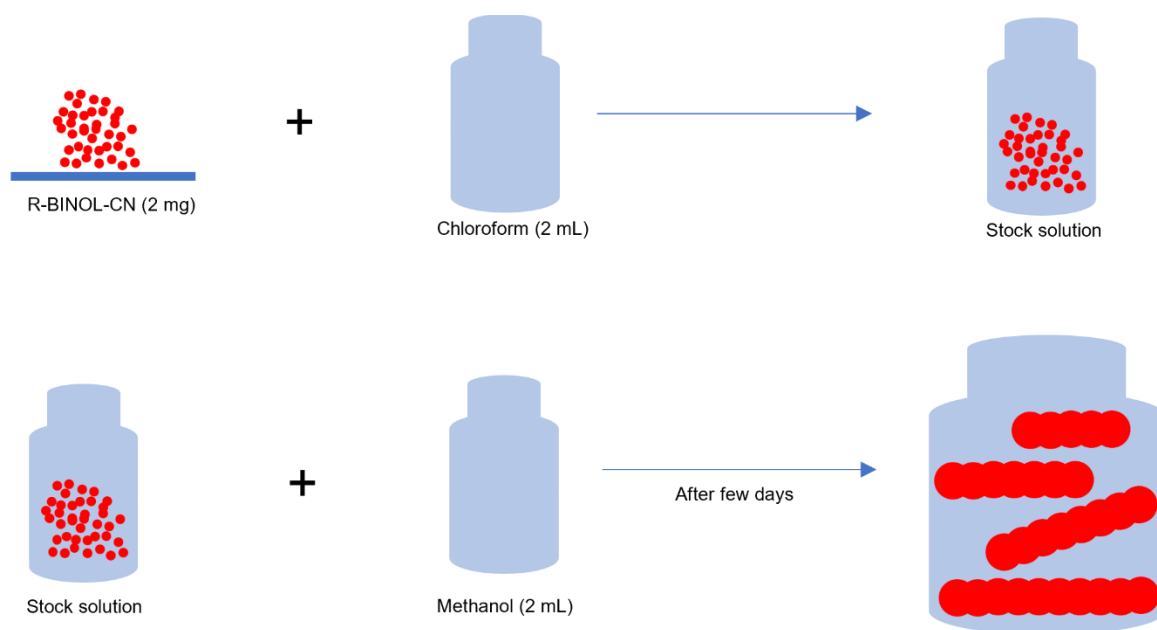


Supplementary Fig. 3: <sup>1</sup>H-NMR spectrum of R-BINOL-CN.



Supplementary Fig. 4:  $^{13}\text{C}$ -NMR spectrum of R-BINOL-CN.

### 1.3 Self-Assembly

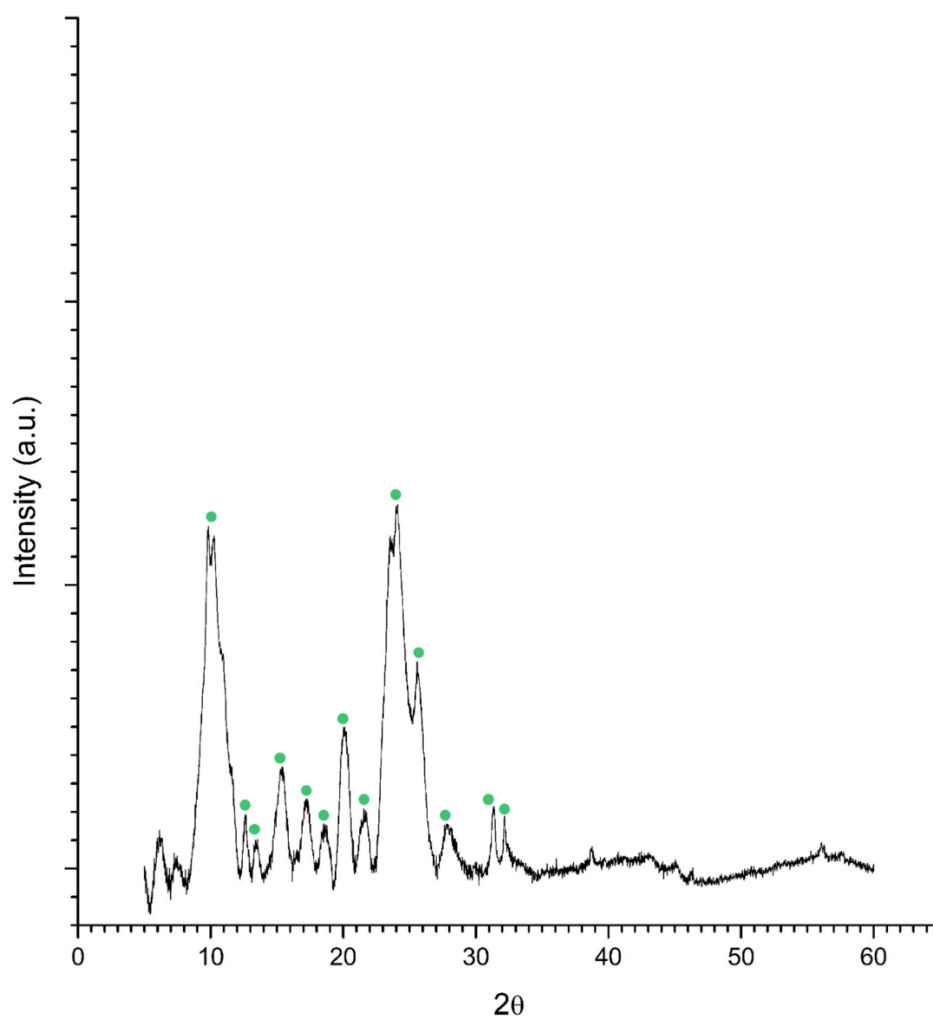


**Supplementary Fig. 5: Schematic of the solution preparation process employed for *ex situ* self-assembly.**

## 1.4 *Ex Situ* Characterisation

### 1.4.1 X-Ray Diffraction (XRD)

X-ray diffraction of the R-BINOL-CN powder was performed on a RIGAKU Ultima IV, fitted with a Cu-K alpha source, operating at a voltage of 40 kV. The scan was performed in the range of 5 to 60 degrees at a rate of 0.5 degree/min with a step size of 0.02 degree. Supplementary Table 1 provides the values of *d*-spacings obtained from powder XRD pattern of R-BINOL-CN.



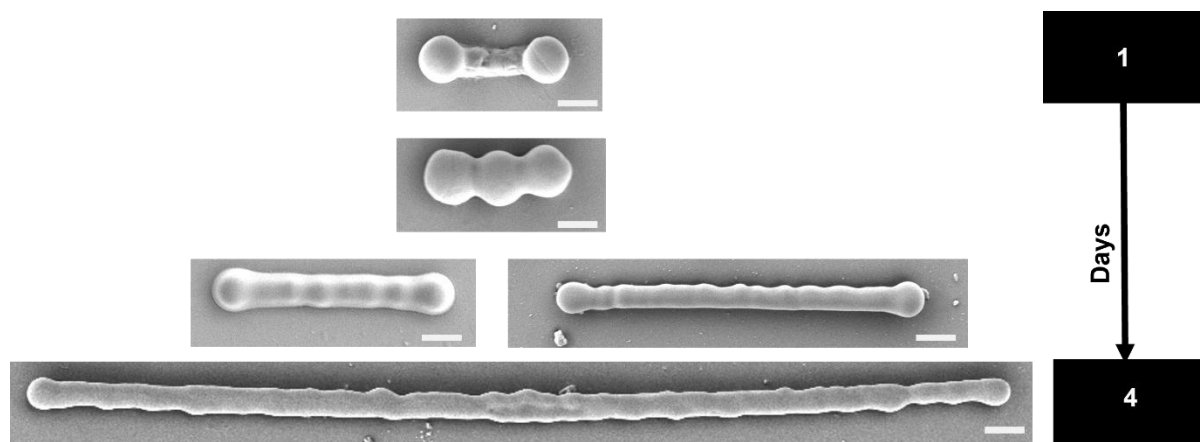
Supplementary Fig. 6: Powder XRD pattern of R-BINOL-CN.

Supplementary Table 1: Values of *d*-spacings obtained from powder XRD patterns of R-BINOL-CN.

<b>2θ</b>	10	12.5	13.5	15.5	17.2	18.7	20	21.7	24	25.7	27.8	31.4	32.2
<b>d (Å)</b>	8.83	7.07	6.55	5.71	5.15	4.74	4.43	4.09	3.70	3.46	3.20	2.85	2.78

## 1.4.2 Field Emission Scanning Electron Microscopy (FESEM)

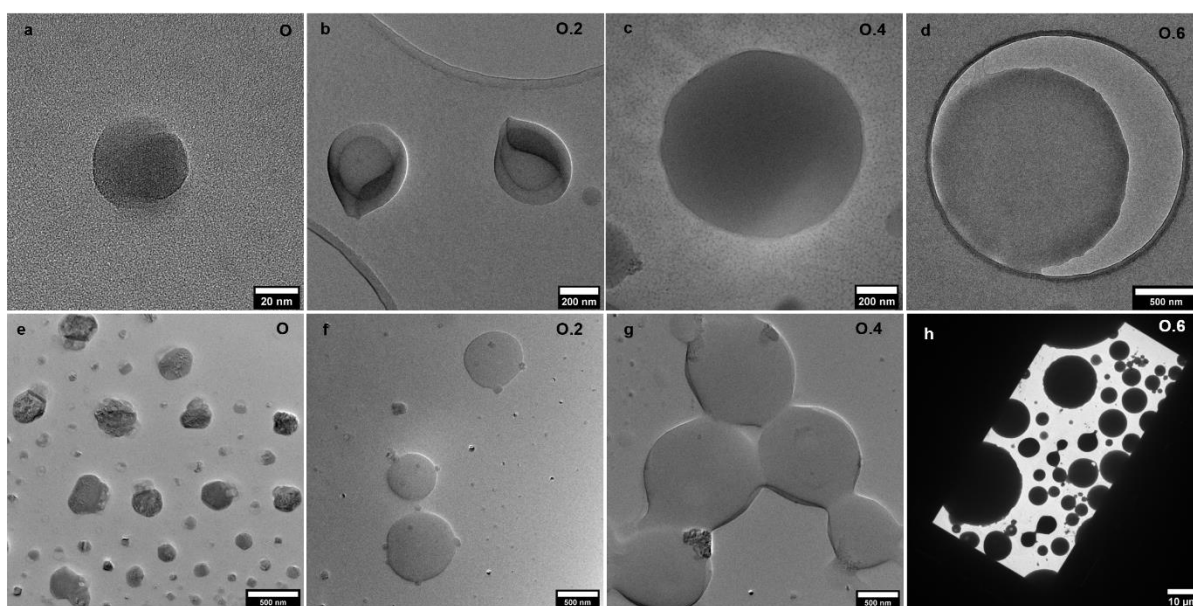
All the FESEM studies were performed on a ZEISS Scanning Electron Microscope operated at an accelerating voltage of 3 kV.



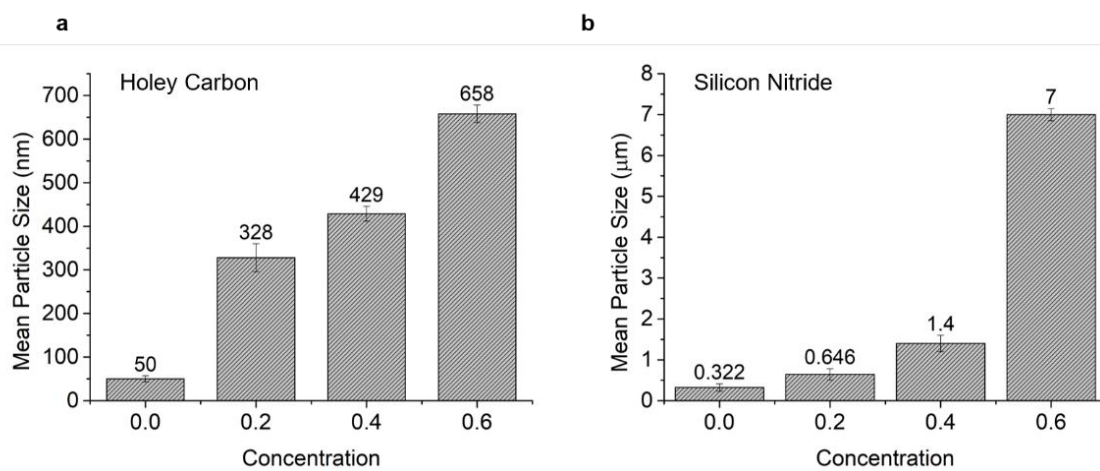
**Supplementary Fig. 7: FESEM images of R-BINOL-CN drop cast on glass coverslips at different time intervals (all scale bars are 2  $\mu\text{m}$ ). Transformations from individual spheres to micropods, and finally into microrods are observed with solution ageing. (The solution used is the same as the one described in the self-assembly section.)**

### 1.4.3 Influence of Substrate on Particle Growth

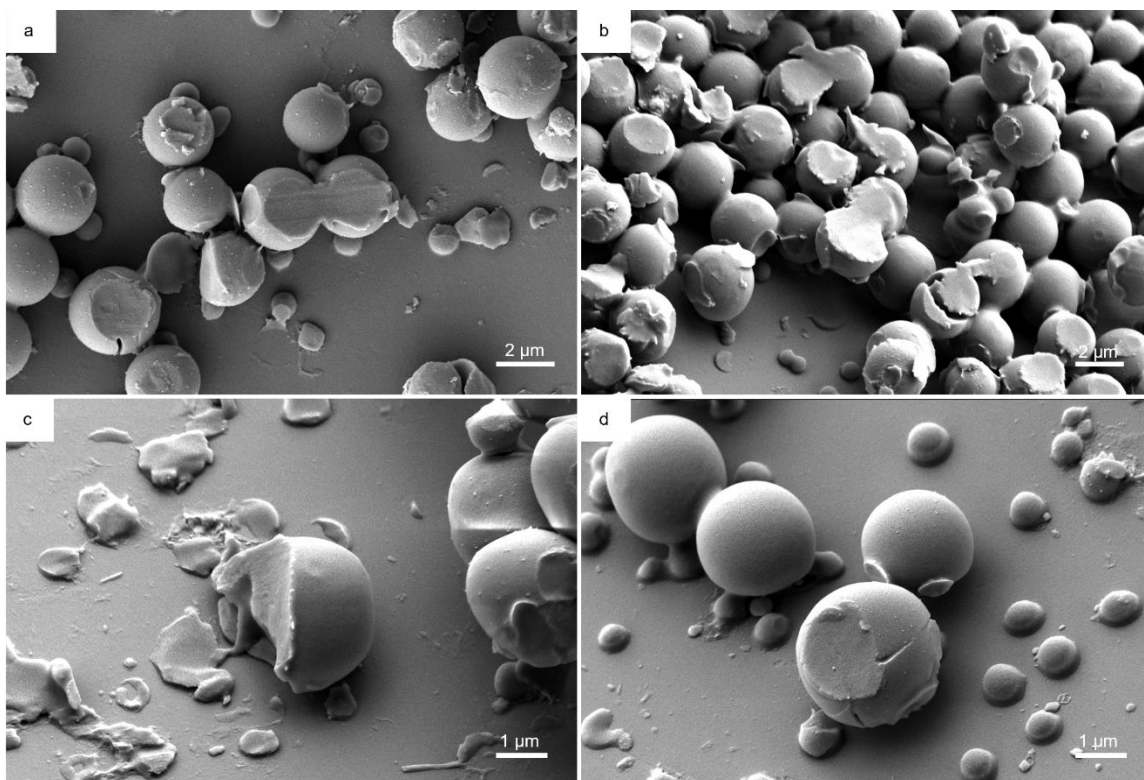
Another essential factor that needs to be considered is the effect of the substrate since surface energies also play a critical role in determining the growth kinetics of particles. It is vital to know how the substrate influences the growth of particles, both in terms of their sizes and shapes, before drawing any conclusions during liquid cell experiments. We performed systematic *ex situ* TEM studies on two types of substrates, namely, holey carbon and silicon nitride, and varied the amount of methanol added. This revealed the size distribution of R-BINOL-CN, allowing us to determine how these substrates facilitated particle growth.



**Supplementary Fig. 8:** TEM micrographs of samples drop-cast on (a-d) holey carbon and (e-h) silicon nitride for different ratios of R-BINOL-CN dissolved in chloroform and methanol (0, 0.2, 0.4, and 0.6).

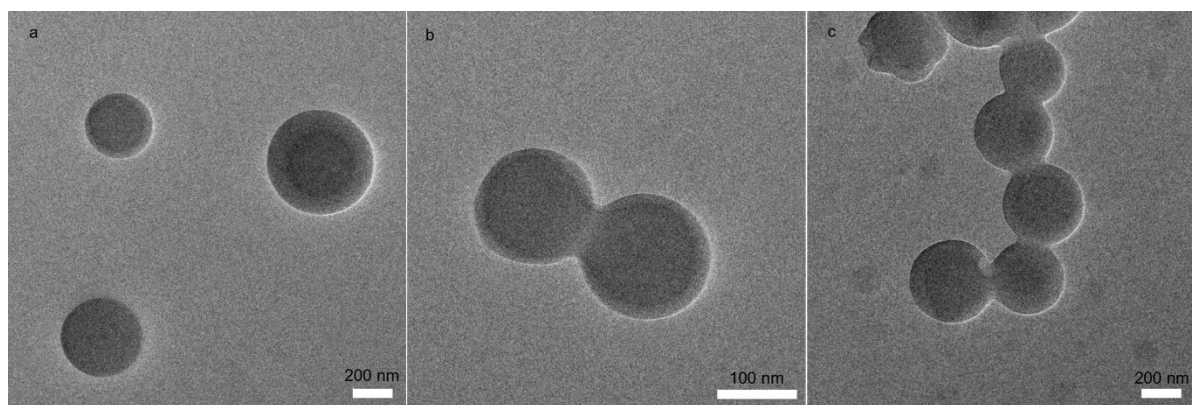


Supplementary Fig. 9: Histogram showing the mean particle size (diameter) for different ratios of R-BINOL-CN dissolved in chloroform and methanol (0, 0.2, 0.4, and 0.6) on (a) holey carbon and (b) silicon nitride substrates.



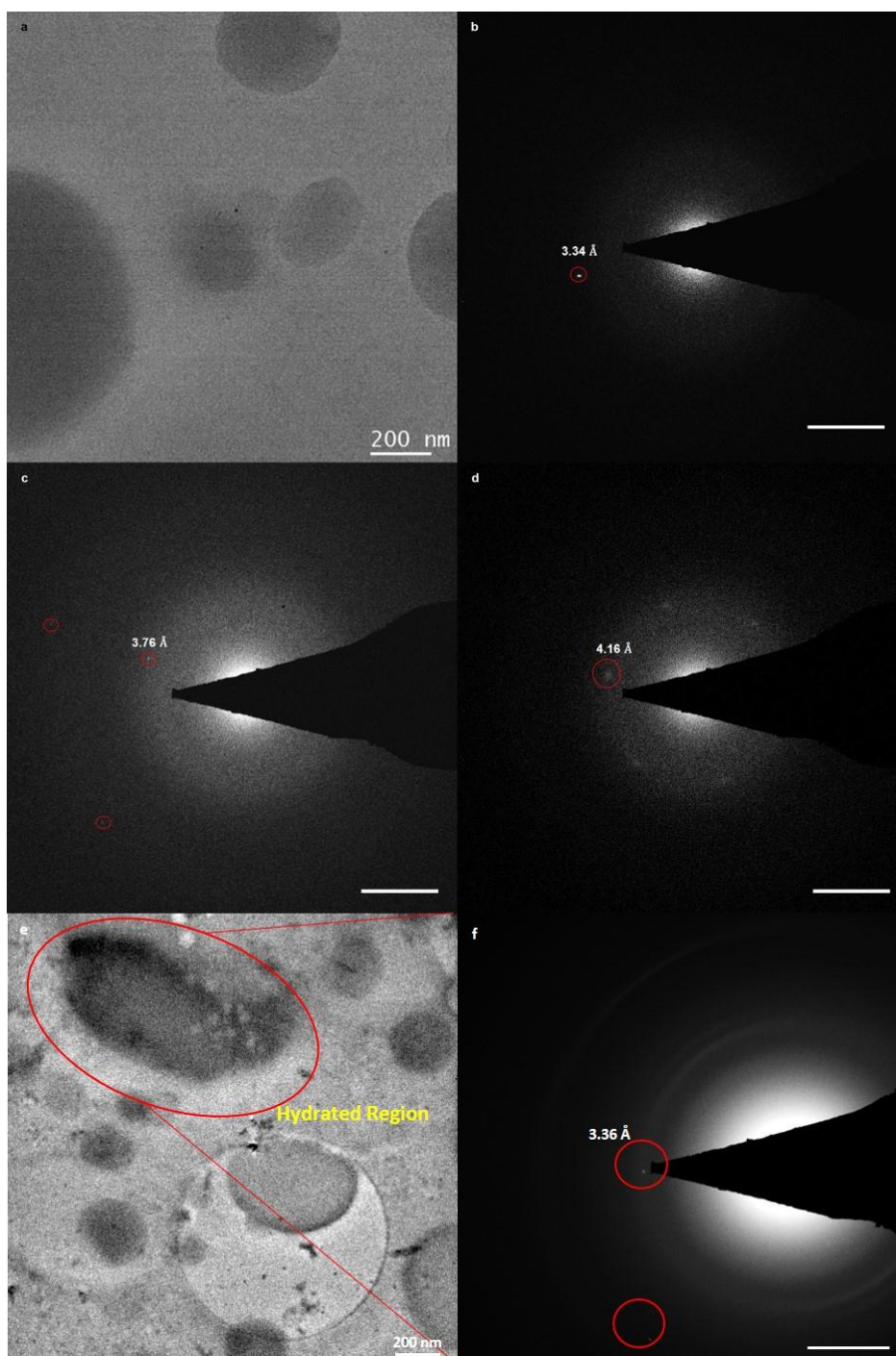
**Supplementary Fig. 10: FESEM images providing evidence that the particles formed are solid spheres.** Imaging was performed on an R-BINOL-CN sample drop cast on a glass cover slip. After the sample dried up, the surface was scratched using a blade to break open the spherical particles. (The solution used is the same as the one described in the self-assembly section.)

#### 1.4.4 Transmission Electron Microscopy (TEM)



**Supplementary Fig. 11: Bright field (BF)-TEM images showing particles formed by drop-casting a solution of ratio 1: 0.6, R-BINOL-CN in chloroform to methanol, on a carbon grid. (a) Individual spherical particles. (b) Two particles forming a neck. (c) Multiple particles are necked together which ultimately form micropods.**

Selected area diffraction patterns (SADP) were obtained from a FEI Titan G2 60-300 HOLO, operated at 300kV, and equipped with a Schottky type high-brightness electron gun (FEI X-FEG), an image  $C_s$  corrector (CEOS) and a Gatan K2 camera.



**Supplementary Fig. 12: Selected area diffraction patterns.** (a) Low-dose Bright field (BF)-TEM image showing particles formed by drop-casting a solution of ratio 1: 0.6, R-BINOL-CN in chloroform to methanol, on a C grid. (b) Corresponding selected area diffraction pattern (SADP) from the near-spherical particles. (c, d) Similar SADP from neighbouring regions. Scale bar for the diffraction patterns is  $2 \text{ nm}^{-1}$ . (e) Bright field image of a Graphene liquid cell (GLC) encapsulating a solution of R-BINOL-CN in chloroform and methanol (1:0.2) (f) Selected area diffraction pattern of R-BINOL-CN particles in the hydrated state obtained at low dose from the region marked by the red circle in (e). Scale bar is  $2 \text{ nm}^{-1}$ .

### 1.4.5 Low-dose 4D-STEM

Low-dose 4D-STEM was performed using a TESCAN TENSOR 4D-STEM operating at 100 kV. The beam current was set to 10 pA, with a beam size of 5 nm, convergence semi angle of 0.5 mrad and a dwell time of 1 ms. The beam current was calibrated on an internal faraday cup. The 4D-STEM scans were 128 x 128 pixels using a 512 x 512 camera frame size. The total deposited dose was calculated to be  $25 e^-/\text{\AA}^2$ .

Dose Calculation:

- Probe current (pA) X electrons per pA = electrons per second

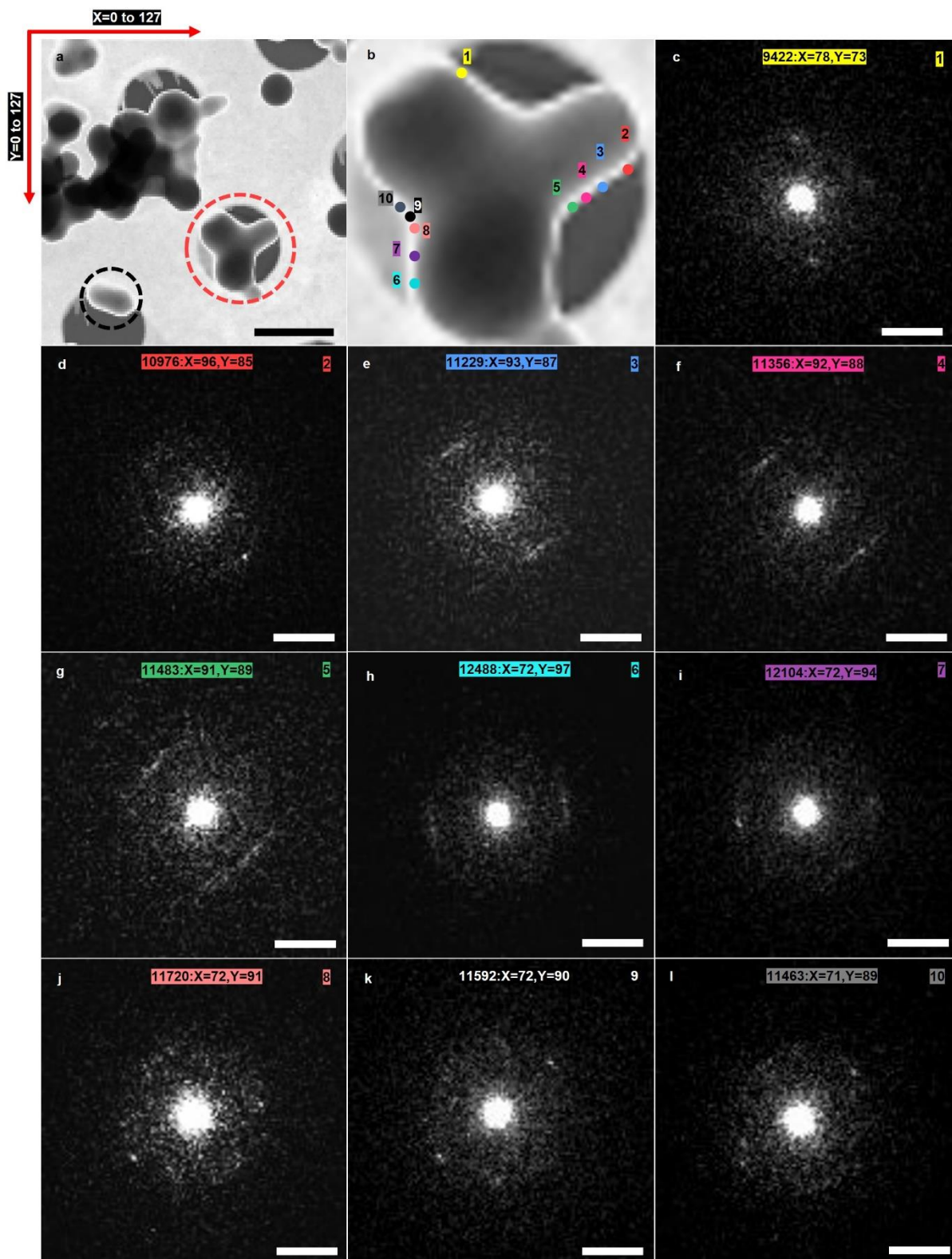
$$(10 \times 10^{-12}) \times (6.242 \times 10^{18}) = 62420000 \frac{e^-}{s}$$

- Electrons per second / Probe area in square angstroms (assumed square) = Electrons per square angstrom per second.

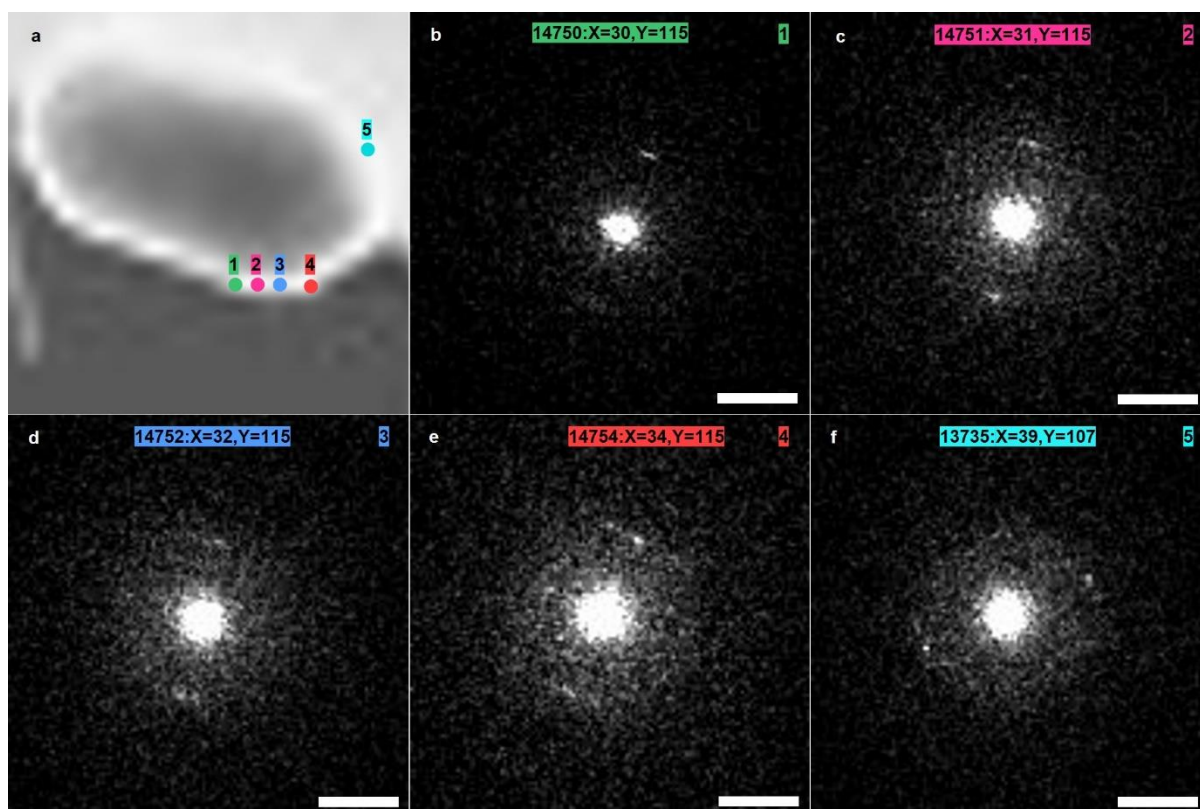
$$\frac{62420000}{50 \times 50} = 24968 \frac{e^-}{\text{\AA}^2 s}$$

- Electrons per square angstrom per second X dwell time in seconds = electrons per square angstrom.

$$D = 24968 \times 10^{-3} = \mathbf{24.968} \frac{e}{\text{\AA}^2}$$



**Supplementary Fig. 13: Low dose 4D-STEM.** (a) VBF STEM image obtained from a specimen of R-BINOL-CN dissolved in chloroform and methanol (in the ratio 1:0.8), drop-cast onto a Cu grid with a holey C supporting film. The region encircled in red shows R-BINOL-CN micropod formed during ASC. The scale bar is 500 nm. (b) Magnified view of the region encircled in red in (a). From low-dose 4D-STEM measurements, diffraction patterns were obtained from every pixel in (a). Diffraction patterns corresponding to points marked 1-10 in (b), from the edge of the micropod, are shown in (c-l). Scale bar here is 10 mrad. A total of 16384 frames were recorded from every pixel in the region shown in (a) and a few of these diffraction patterns obtained from the edge of the micropod are labelled by their coordinates and TIFF frame number from the entire dataset that has been provided.



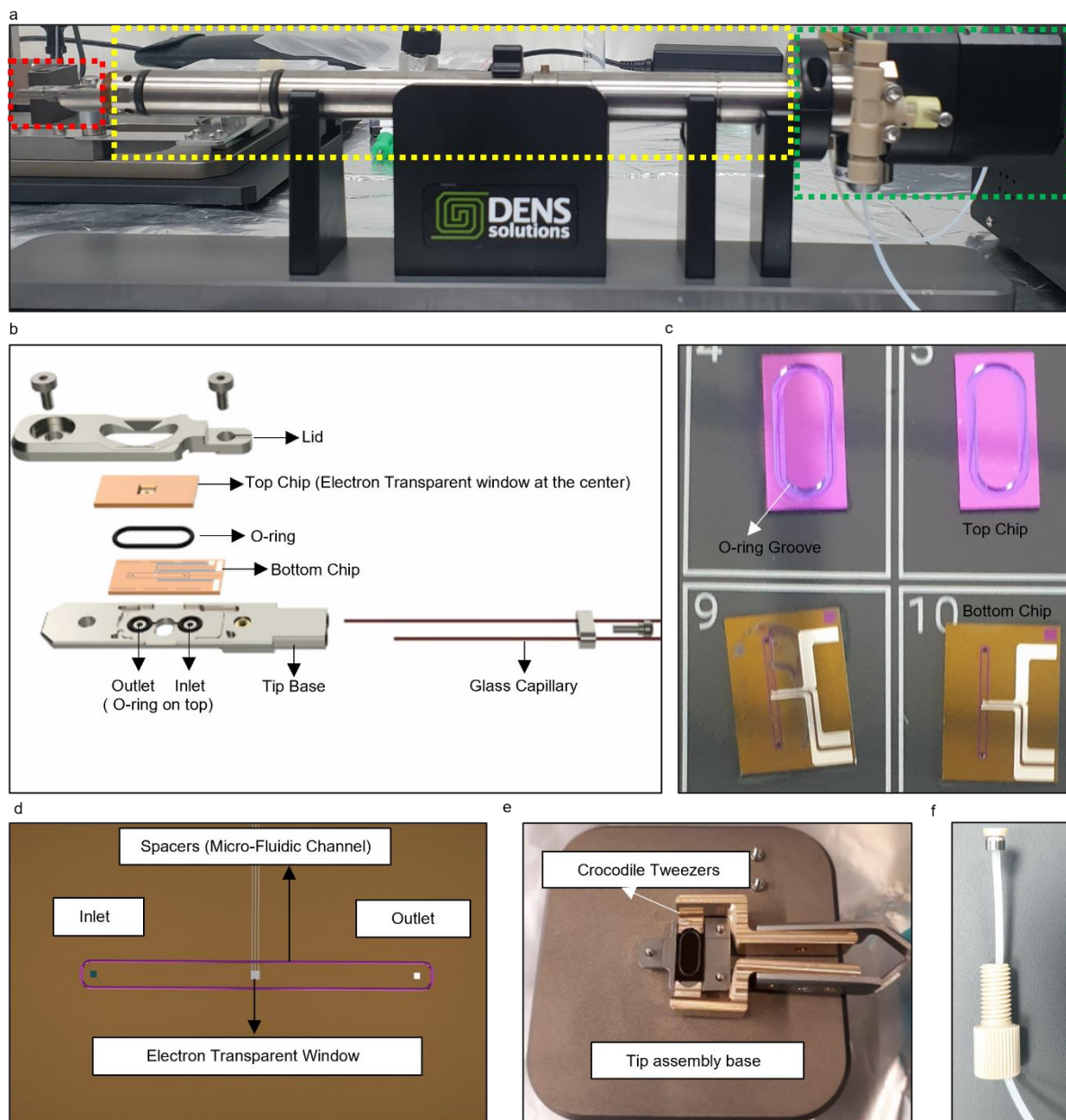
**Supplementary Fig. 14: Low-Dose 4D STEM.** (a) Magnified view of the black dotted region in Fig 9a. (b-f) Diffraction patterns corresponding to points marked 1-5 in (a), from the edge of the R-BINOL-CN particle. Scale bar is 10 mrad.

## Supplementary Note 2

### 2 Methods

#### 2.1 Holder Design

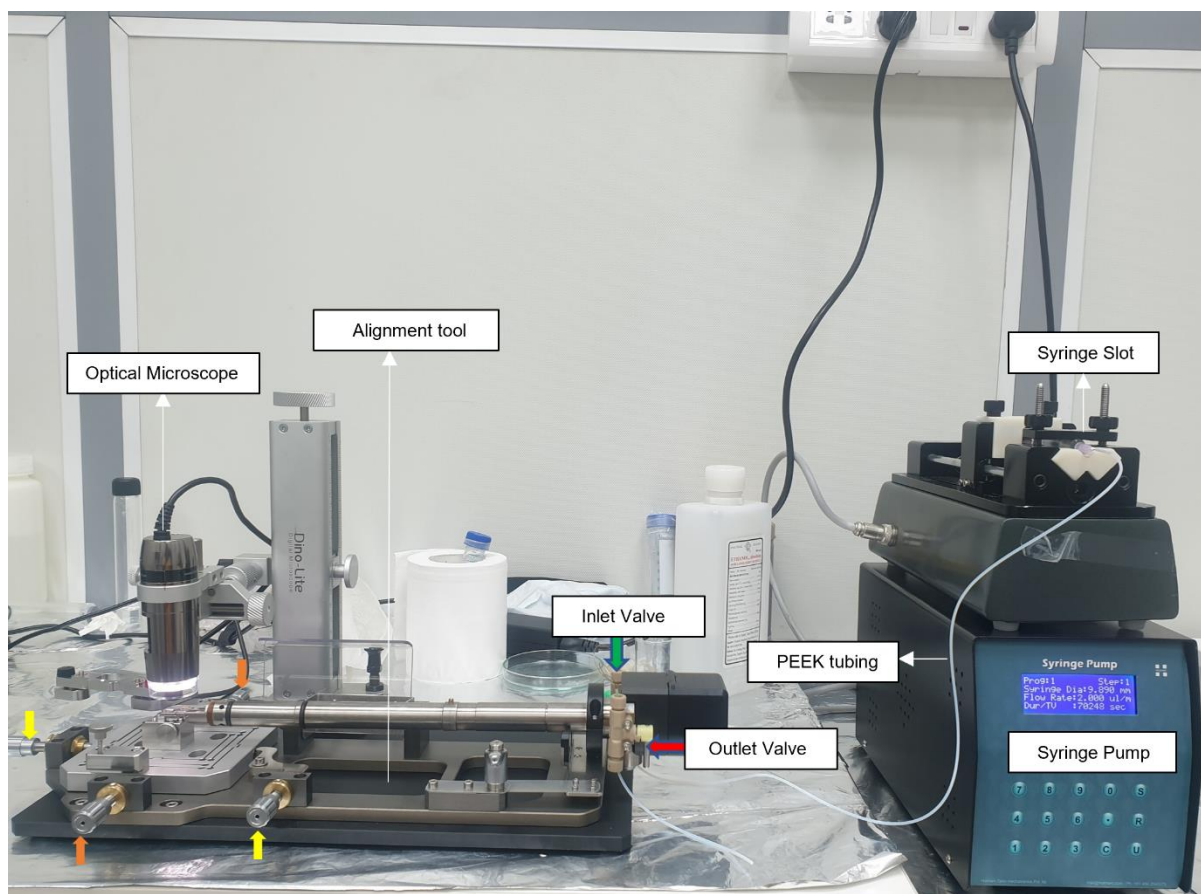
All the experiments were performed using the DENSolutions Stream Holder compatible with a JEOL transmission electron microscope (F200). The holder comprises three sections, namely, the back part, the shaft, and the tip where the liquid cell is placed.



**Supplementary Fig. 15: Various components of the DENSolutions Stream System. (a)** Photograph of the Stream holder showing the back part (green dotted box), shaft (yellow dotted box), and tip (red dotted box). **(b)** Exploded view of the holder tip showing the different components (configuration looks slightly different for a JEOL holder). **(c)** Photograph of the top (upper) and bottom (lower) chips used in the experiments. **(d)** Overview of the bottom chip consisting of a microfluidic channel defined by the spacers, which directs the flow from inlet to outlet. **(e)** Photograph of tip assembly base provided with the holder. **(f)** PEEK tubing and PEEK fitting is used to interface the syringe pump to the holder.

## 2.2 Nano-Cell Design & Chip Assembly

The tip holds a dual-chip liquid Nano-Cell formed by sandwiching two MEMS devices to create a tiny, sealed chamber (Supplementary Fig. 15b). This Nano-Cell configuration consists of a top chip and a bottom chip (Supplementary Fig. 15c). The bottom chip has an integrated inlet and outlet as well as spacers (200 nm) which define a microfluidic channel (Supplementary Fig. 15d). Both chips have rectangular electron transparent windows (approximately 20  $\mu\text{m}$  (width) x 200  $\mu\text{m}$  (length) which when aligned on top of each other allow the beam to pass through; See Supplementary Movies 6 and 7). To assemble the Nano-Cell, the bottom chip was placed on the liquid inlet and outlet holes present on the tip base, with O-rings around them providing a leak-proof seal. A tip assembly base supplied along with the holder was used to mount the top chip onto the bottom one (Supplementary Fig. 15e). The top chip was first placed on the lid of the tip. A Viton O-ring was then inserted into the groove provided on the top chip to ensure that the Nano-Cell is leak tight. The lid and the top chip were then lifted together using crocodile tweezers and mounted on the tip. The whole assembly was fastened with the help of screws. At this stage, the holder was placed onto the alignment tool to create an overlap between the electron transparent windows on the top and bottom chips so that the electron beam can penetrate. Once the windows were aligned, the inlet valve on the back of the holder was connected to the syringe pump using PEEK tubing. A 1.8mM solution was prepared by adding 1 mg of R-BINOL-CN in 1 ml of chloroform. This solution was transferred into a 5 ml glass syringe and fitted onto the syringe pump. The entry of liquid into the cell was spotted using the optical microscope on the alignment tool.

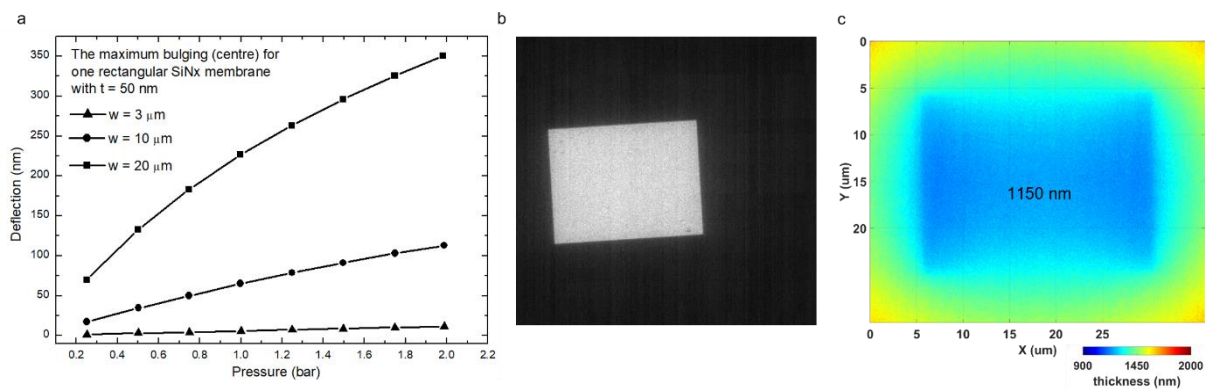


**Supplementary Fig. 16: Photograph of the holder connected to the syringe pump.** After mounting the tip onto the holder, it was placed on the alignment tool fitted with an optical microscope, and the electron transparent windows on the top and bottom chips were aligned using the X (yellow arrow) & Y (orange arrow) adjustment screws. A syringe pump was connected to the inlet valve on the backside of the holder using PEEK tubing. The solution containing R-BINOL in chloroform was introduced using this configuration, where the optical microscope helped to monitor the entry of fluid into the cell.

## 2.3 Liquid Flow

The liquid can be introduced into the viewing area of the liquid cell by using either a syringe pump or a pressure-based pump. In our case, all the experiments were performed at static fluid conditions. Particularly, antisolvent precipitation occurs instantaneously the moment methanol mixes with the solution containing R-BINOL-CN dissolved in chloroform. Therefore, this process is independent of the rate of fluid flow and does not necessitate a continuous flow of methanol. Thus, we chose to use a syringe pump at its lowest possible flow rate (2  $\mu\text{L}/\text{min}$ ). However, based on experimental demands, this holder is compatible with a pressure-based pump that can provide a continuous flow of liquid at very low flow rates. To facilitate fluid flow, the back part of the holder has two manual valves at the sides. The inlet and outlet valves regulate the entry and exit of liquid into the holder. We connected the syringe pump to the inlet valve via PEEK tubing of 300  $\mu\text{m}$  internal diameter. From here, glass capillaries connected using PEEK fittings run through the shaft, into the tip of the holder, and lead the fluid into the liquid cell placed at the tip. The fluid exits the holder also via the glass capillary connected to the outlet valve. The major advantage of the liquid cell design of the Stream holder, as compared to other commercially available solutions, is the presence of an on-chip channel which facilitates a controlled flow (See Supplementary Movies 8, 9, and 10). This design makes it possible to either push or pull liquid within the field of view. However, due to high fluidic resistance in the channel, it is difficult to have real control over the flow rate.

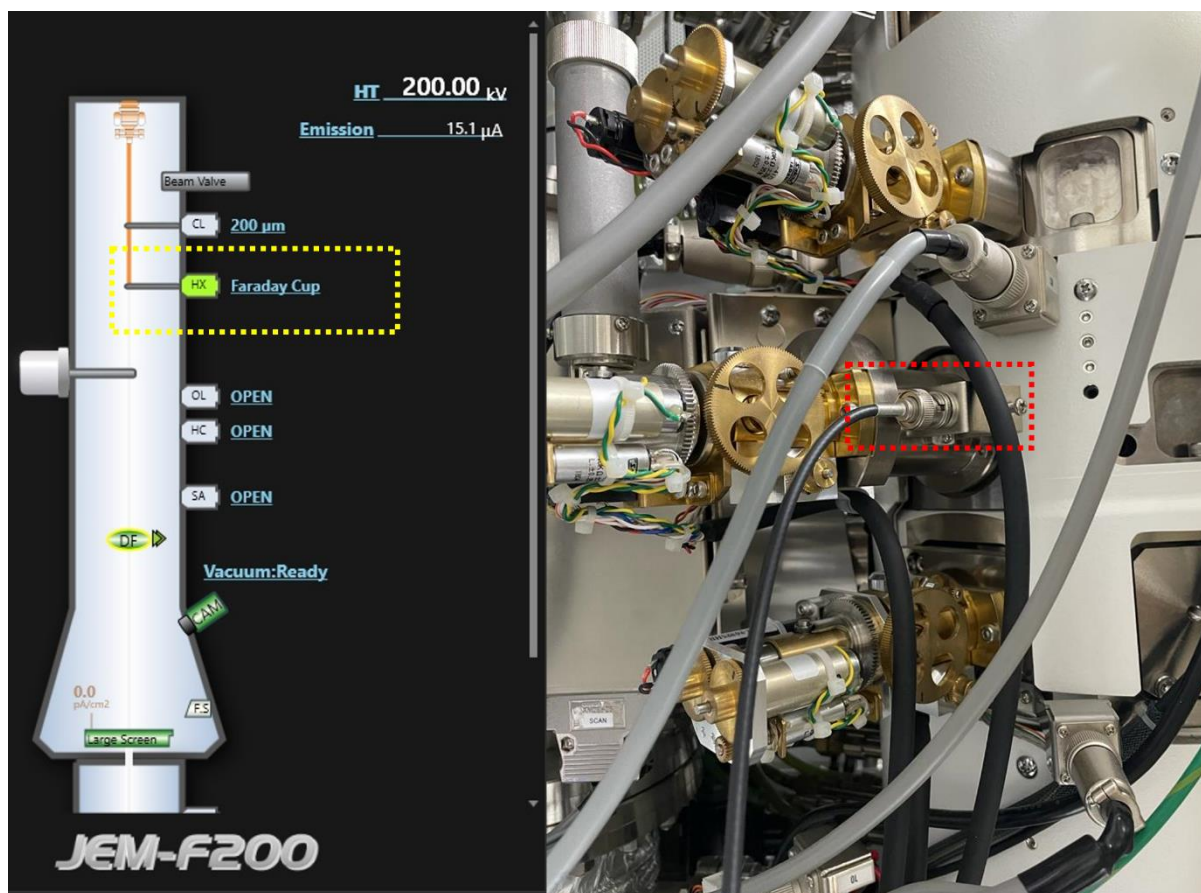
All other commercially available liquid cell holders use a bathtub-type design where the fluid first enters a well in which the chips are placed. Since the area around the chips offers a lower fluidic resistance, the flow entirely bypasses the chips<sup>[31]</sup>. Hence, one must completely rely on diffusion to bring the liquid into the viewing area. However, in all the MEMS-based chips, the silicon nitride windows undergo bulging due to the pressure difference between the inside of the Nano-Cell and the column of the microscope. This could alter the overall liquid thickness through which imaging is carried out, and in turn the achievable contrast. Thus, window bulging must be considered while performing experiments using liquid cells.



**Supplementary Fig. 17: Bulging of silicon nitride windows. (a)** Plot showing the range of deflection in silicon nitride window of 50 nm thickness as a function of the pressure difference between the inlet and outlet while using a pressure-based pump. In our experiments, we used a syringe pump where the pressure difference was 1 bar. The bulging depends on the width ( $w$ ) of the window used. **(b)** Bright-field TEM image of Nano-Cell assembly without any liquid. **(c)** Simulated image showing bulging across different regions of an empty Nano-Cell assembly when the inlet and outlet valves are closed. The bulging at the centre was estimated to be 1150 nm.

## Supplementary Note 3

### 3 Electron dose



**Supplementary Fig. 18:** Photograph of the microscope column showing the slot (red dotted box) for connecting the pico-ammeter. The faraday cup is positioned below the condenser aperture (shown by the yellow dotted box).

The electron dose used for the experiments performed on the JEOL F200 was measured using a Faraday cup provided with the microscope. By connecting a pico-ammeter to the microscope (red dotted box) and inserting the Faraday cup positioned near the hard X-ray aperture (yellow dotted box), we measured the STEM probe currents. Dose optimisation was performed based on the minimum necessary dose to nucleate particles during the experiment performed on a solution containing R-BINOL-CN dissolved in chloroform (1.8 mM). In this study, we tried to nucleate R-BINOL-CN particles by parking the STEM probe for 2-3 seconds. We established the minimum dose requirements by starting from the smallest possible spot size (10) and different aperture sizes. By following this approach, we observed that a combination of spot size 5 and 40  $\mu\text{m}$  aperture gave us the minimum current (0.054 nA) needed to nucleate R-BINOL-CN particles at this concentration. Therefore, we used this dose value for the experiment (Supplementary Movie 5 and 6) performed in the absence of methanol. We failed to nucleate particles at spot sizes less than 5 despite parking the

probe for longer durations ( $\sim 20 - 30$  s). For experiments on antisolvent crystallization and oriented attachment (Supplementary Movies 2, 4, and 7), we operated at nearly four times lower probe currents (0.013 nA) to minimize the effects of the electron beam on the growth process. Table 2 provides the values of probe currents ( $i_e$ ) for different spot and aperture sizes.

**Table 2: STEM probe current (nA) measured at various combinations of aperture and spot sizes.**

Spot Size	Aperture ( $\mu\text{m}$ )		
	200	100	40
5	1.360	0.360	<b>0.054</b>
6	0.704	0.179	0.027
7	0.359	0.091	<b>0.013</b>

The electron dose ( $e^-/\text{\AA}^2$ ) was calculated using the electron beam current, pixel dwell time and pixel size. We calculated the dose per frame by dividing the probe current at the sample,  $i_e$  (C/s), by the scan area  $A$  ( $\text{\AA}^2$ ) and multiplying by the frame time ( $t_f$ ) as follows:  $(i_e \cdot t_f)/e \cdot A$  ( $e$  is the elementary charge, C/electron and  $t_f=2.16$  s).

**Table 3: Values of electron dose ( $e^-/\text{\AA}^2$ ) for capturing the STEM movies.**

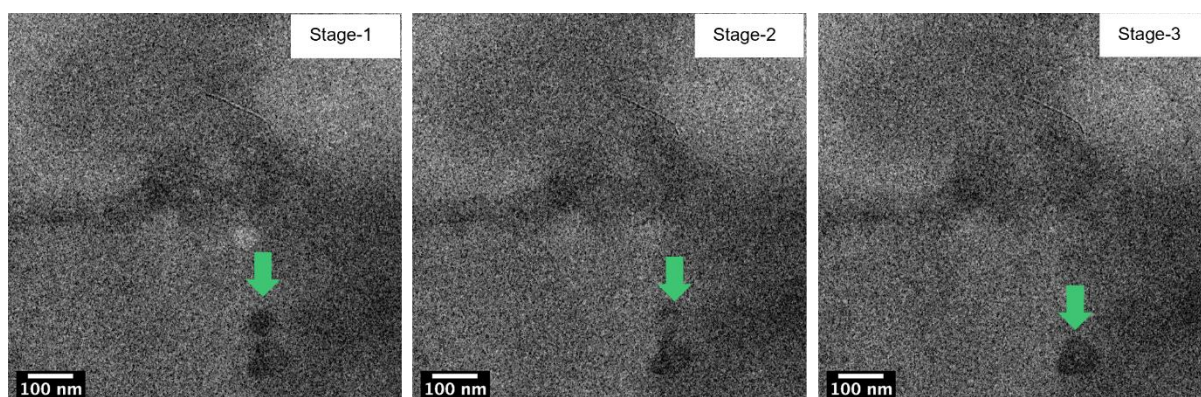
Supplementary Movie No	Probe Current (nA)	Scan Area(A)	No of Frames	Dose per frame ( $e^-/\text{\AA}^2 \cdot f$ )	Total Dose ( $e^-/\text{\AA}^2$ )
2	0.013	13x13 $\mu\text{m}^2$	114	0.01	1.18
4	0.013	10x10 $\mu\text{m}^2$	100	$\sim 0.01$	1
5	0.054	16x16 $\mu\text{m}^2$	78	0.028	2.22
6	0.054	19 x19 $\mu\text{m}^2$	279	0.020	5.58
7	0.013	248x248 $\text{nm}^2$	213	28.53	6077.89

## Supplementary Note 4

### 4 *In Situ* Liquid Cell Trials

#### 4.1 Graphene Liquid Cells (GLCs)

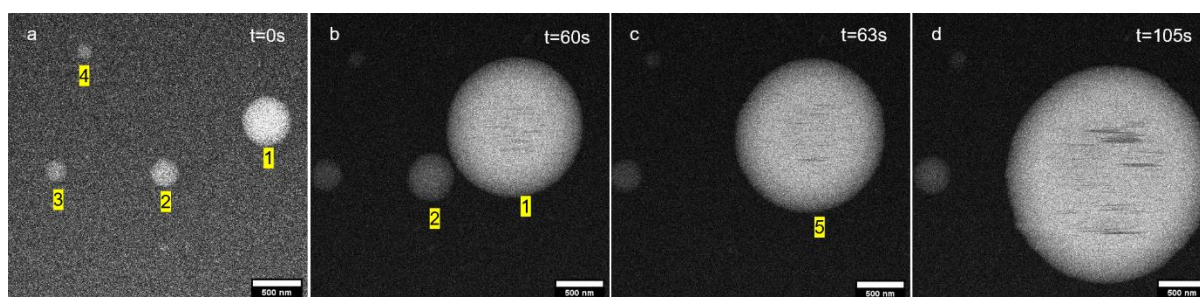
Results from the systematic *ex situ* studies, using both TEM and FESEM, indicated that precipitation of particles occurs due to the addition of methanol to the solution containing R-BINOL-CN in chloroform. Hence, the experimental tool (holder) for performing these experiments using *in situ* TEM techniques should be capable of mixing two different solutions within the viewing area of the microscope. However, before proceeding to this step, we performed some trial *in situ* liquid cell experiments on premixed solutions of R-BINOL-CN in chloroform and methanol using graphene-based liquid cells (GLCs). Through these studies, we intended to capture the growth dynamics of R-BINOL-CN at a very early stage, when the particles are still in the nanometer size range. Based on the *ex situ* TEM observations, we prepared a solution by mixing a suitable amount of methanol (0.1 : 1) into the stock solution of R-BINOL-CN in chloroform, such that particles of sizes 50 - 100 nm could precipitate. A small volume (1  $\mu\text{L}$ ) of this solution was placed on a graphene-coated holey carbon grid and an identical grid is placed on top of it. This encapsulated the solution in between two graphene layers, thereby forming sealed liquid pockets ranging from 50 - 400 nm in size<sup>[53]</sup>. This grid assembly was then introduced into the microscope for imaging. The experiments were performed on a JEOL 2100 microscope, with a LaB6 emitter operating at 200 kV. A liquid pocket was identified, and the growth of R-BINOL-CN particles was followed by imaging in TEM mode. We observed two particles fusing via three subsequent stages. In the first stage, the two particles approached each other, followed by their surfaces coming in contact, finally resulting in their fusion into a single particle.



Supplementary Fig. 19: Snapshots from a BF-TEM movie showing various stages in the fusion of R-BINOL-CN particles within a liquid pocket of a graphene liquid cell.

## 4.2 DENSsolutions Ocean Holder

All the initial liquid cell holders based on dual MEMS chips utilised a bathtub design for introducing liquid into the viewing area of the Nano-Cell. There are a few studies in literature where liquid mixing experiments were performed using these holders. Therefore, we tried to investigate the possibility of employing such a holder (DENSsolutions Ocean) for elucidating the antisolvent precipitation process occurring during the mixing of two volatile solvents. Before performing the mixing experiment with two solvents, we ran preliminary tests using a single liquid. These trials were necessary to gauge the liquid layer thickness and, thereby, the contrast obtained while imaging. A 1.8mM solution of R-BINOL-CN dissolved in chloroform was used to follow the kinetics of particle growth in the absence of methanol. These experiments were performed at 300 kV on a Titan 80-300 STEM equipped with a high-brightness Schottky field emission electron gun. The energy of the electron probe was used to nucleate the particles. The electron beam-mediated nucleation is explained using various theories, such as the creation of electric fields by the incident electron beam and localised heating which can cause a concentration of ions resulting in a local supersaturation in the area of illumination or leading to a reduction in the free energy of the solution and change in parameters like pH of the solution due to radiolysis interactions which possibly modify the energy barrier necessary for crystallisation<sup>[54]</sup>. The snapshots from the STEM time series (Supplementary Movie 12) show the growth of particles (Supplementary Fig. 20). We see that particles 1 and 2 initially grow via monomer attachment ( $0 < t < 60$ s), after which they coalesce together to form a larger particle 5 ( $t=63$ s). The larger particle 5 continues to grow ( $63 < t < 105$ s), before finally disappearing from the field of view. These experiments also provided us with evidence that STEM parameters like dwell time, spot size, and aperture size influenced the growth process. Due to the liquid cell design, the flow of liquid into the viewing area is solely reliant on diffusion. This meant that there was no way to control either the flow or the liquid layer thickness. Therefore, we had to repeat this experiment several times to achieve good contrast in the STEM movies, despite using only a single liquid (Supplementary Movie 11).



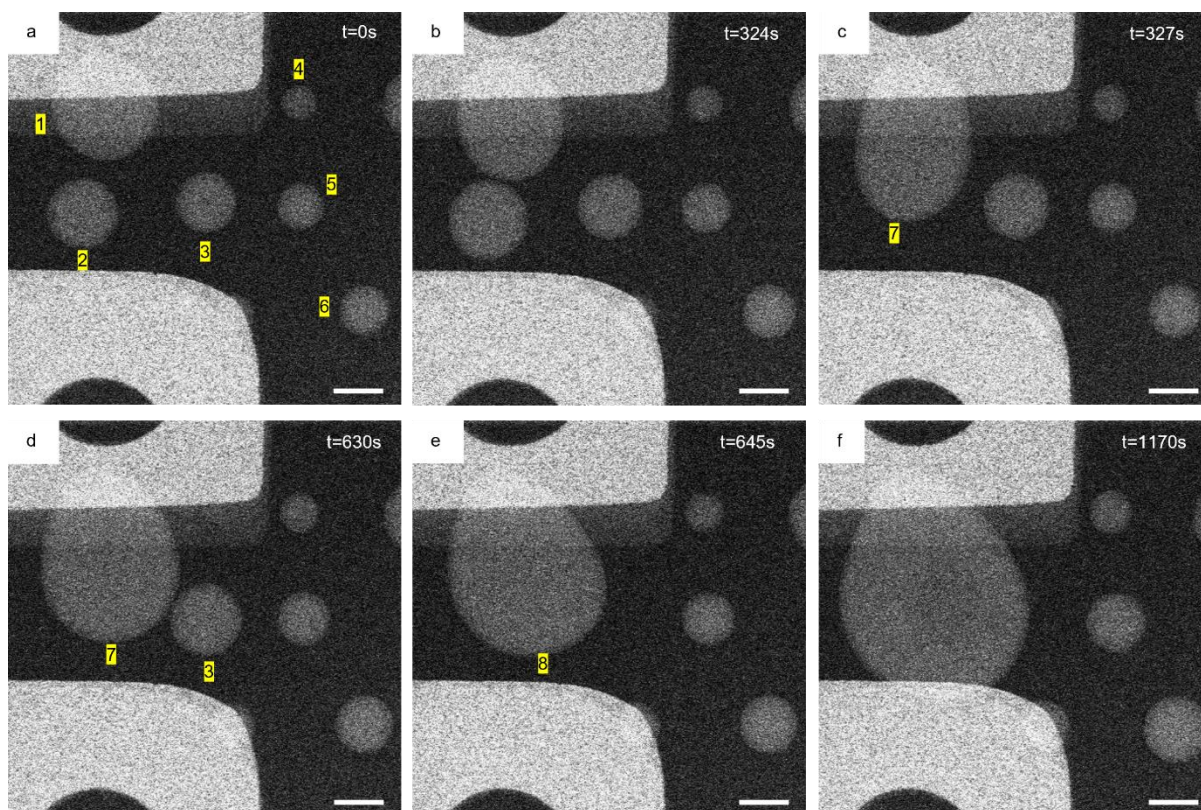
**Supplementary Fig. 20: Snapshots from an ADF-STEM movie (Supplementary Movie 12) captured using the Ocean Holder. (a-d)** The various stages of growth of R-BINOL-CN particles with time. All scale bars are 500 nm.

After completing these trials, experiments on anti-solvent crystallisation were attempted. One of the previous studies on mixing liquids using the Ocean holder made use of a straightforward drop casting technique<sup>[22]</sup>. Here, the first solution was drop cast on the silicon nitride window of the bottom chip. Then the top chip was placed above the droplet, and the cell was assembled. The second liquid was then flowed into the holder using a syringe pump. However, this way of mixing could not be adopted for our experiments due to the extremely volatile nature of the solvents. It was seen that a small droplet of R-BINOL-CN dissolved in chloroform dried up in less than 10 seconds. It is practically not possible to assemble the chips and align the windows within this timeframe. Therefore, this method was unsuitable for experiments involving volatile solvents.

The other study used air to push the excess first solution left within the area of the bathtub<sup>[20]</sup>. Once the bathtub area was emptied, the second solution was introduced into the holder. Firstly, using air to push the excess liquid in our case resulted in the evaporation of chloroform that diffused in between the chips. This caused the liquid in the viewing area to also dry up. Secondly, there is no way to detect if all the excess chloroform is pushed out of the bathtub, which leads to the possibility of liquid mixing taking place outside the viewing area itself. Since anti-solvent precipitation occurs instantaneously, it is pivotal that methanol interacts with the chloroform only inside the viewing area to be able to have any chance of capturing this process. We made several attempts to introduce methanol using this approach but were unsuccessful in visualising the process. Thus, the Ocean holder was deemed unsuitable for carrying out anti-solvent precipitation, and instead, we chose to use the Stream holder.

### 4.3 DENSsolutions Steam Holder

Preliminary trials were conducted on the solution containing R-BINOL-CN dissolved in chloroform (1.8 mM) to understand the growth of R-BINOL-CN particles in the absence of methanol and to tune the electron dose. By operating the microscope in STEM mode, we nucleated several particles by parking the electron beam at different locations for 2-3 seconds. A dwell time of 1  $\mu$ s was used. The snapshots from a time series (Supplementary Movie 13) show the growth kinetics of particles labelled from 1-6 (Supplementary Fig. 21a). With time, a significant increase in the sizes of particles 1 and 2 was observed (t=324s) due to growth via monomer attachment. As their surfaces met each other, they coalesced to form a single large particle (t=327s). This particle continued to grow again via monomer attachment until it encountered particle 3 (t=630s), which resulted in another coalescence event (t=645s). We observed that particle 8 further increased in size and ended up having a pear-shaped morphology (t=1170s). We used these experiments as a reference to optimise the experimental parameters like dwell time, aperture size, spot size and volume of liquid inside the cell affect particle formation. This was a critical step in performing experiments in a controlled way.



**Supplementary Fig. 21: Snapshots from an ADF-STEM movie (Supplementary Movie 13) captured using the Stream Holder. (a-f) The various stages of growth of R-BINOL-CN particles with time. All scale bars are 1  $\mu$ m.**

## Supplementary Note 5

### 5 Data Analysis

The data analysis was performed using FIJI/Image J<sup>[55-57]</sup> as well as in-house PYTHON scripts. All the images were recorded in STEM mode, with a size of 512 x 512 pixels, and using a dwell time of 5  $\mu$ s. The time interval between the two frames was estimated by dividing the total time (calculated from the time stamps on the 1<sup>st</sup> frame and 50<sup>th</sup> frame obtained from the image) it took to record the series by 49. This resulted in a time of 2.16 s in between each frame, consistent across all the experiments.

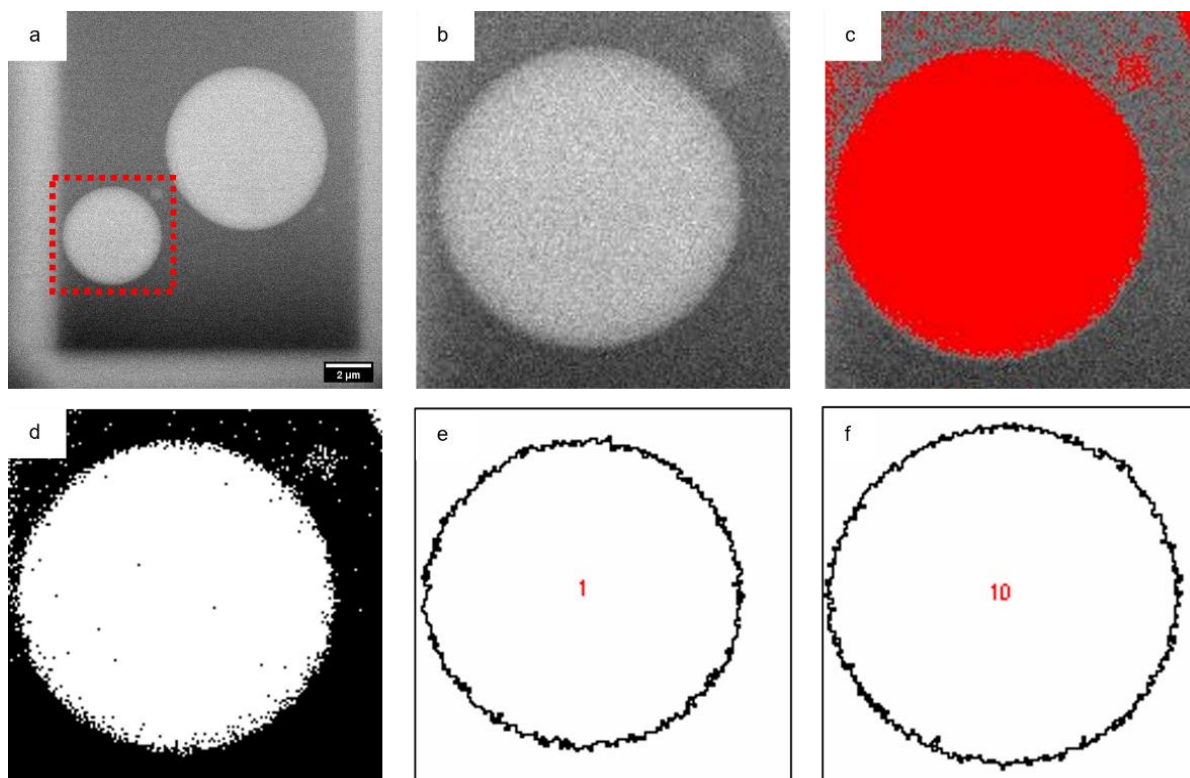
We used FIJI/Image J to create movies from the STEM images. The image sequences from each of the experiments were imported and saved as 32-bit TIFF stacks. Then background variation between different frames was corrected for all the movies by using the following procedure. (i) First, the image stack is duplicated. (ii) Then the size of this duplicate stack is changed from 512 x 512 to 1 x 1 pixels and back again to 512 x 512. By performing this step, the intensity of the image stack is normalised and averaged across all the frames. (iii) Next, the original stack is divided by this duplicated stack (Process-Image calculator) to obtain a new background-corrected 32-bit stack with improved contrast. All further analysis was done on these background-corrected stacks.

#### 5.1 Determining Growth Rate of Particles - Experiments without Methanol

The change in the area of particles with time must be known to estimate the kinetics of particle growth. We used FIJI/Image J to determine the area of the particle from each frame of the movie. Below, we describe the procedure employed for estimating the area of particles in Fig. 4. In this case (Supplementary Movie 4), the growth of particles for 10 frames was followed.

- First, the region around the particle was cropped out from the entire frame.
- The threshold is then adjusted to cover the area of the particle to be measured (red colour). Once the area is marked, the threshold is set.
- Next, the “Analyse Particles” option was used to automatically generate a bare outline map of the particles for all 10 frames of the image stack, marking the area covered by the particle.

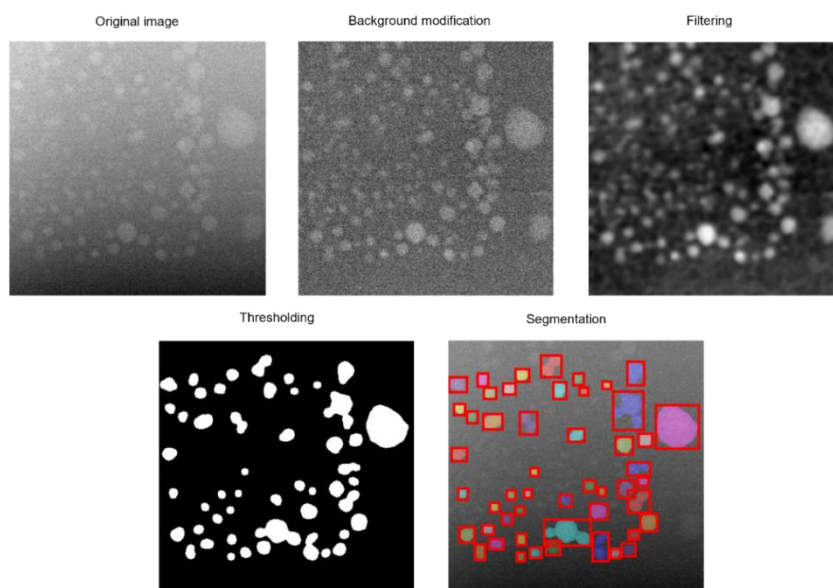
The results were obtained in a tabular form, with the area of the particle displayed in pixels, which can be exported in a desired file format. From the area values  $A$ , the radius of the particle  $r$  in each frame was calculated by using the formula  $A = \pi r^2$ . Since the scale bar is known, the radius values were converted to units of length ( $\mu$ m). A similar procedure was used to determine all the growth rates.



**Supplementary Fig. 22: Various steps involved in extracting the area of a particle using FIJI/Image J. (a)** Original image stack with two particles within the field of view. **(b)** Particle of interest cropped out (red dotted box). **(c)** The threshold adjusted to highlight the particle area. **(d)** Threshold set. **(e-f)** The bare outline of particles from frames 1 & 10 respectively, obtained using the “Analyse Particles” feature.

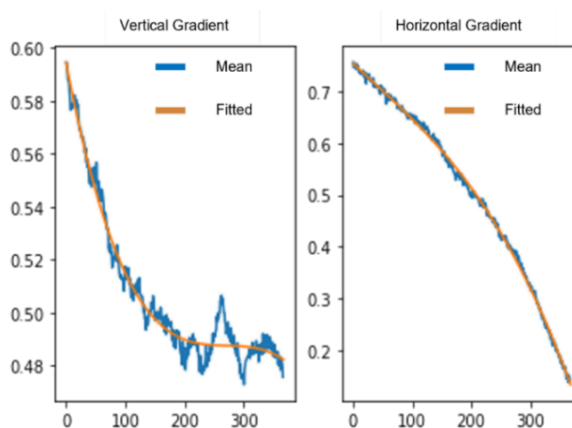
## 5.2 Statistical Analysis and Growth Rate of Particles - Antisolvent Crystallisation

The image processing of the video series (Supplementary Movie 2) for statistical analysis was performed in 4 steps.



### I. Background modification

The left top corner of the original image was brighter than the right bottom corner, which might be caused by the unevenness of liquid cell thickness during the reaction. The mean intensity of the vertical and horizontal direction of the image was plotted (blue). A polynomial function of degree three (orange) was applied to fit the vertical and horizontal mean gradation. Each pixel intensity of the image was edited based on these two fitted cubic functions. All edited intensity values of each image were adjusted within the 0 to 1 range.

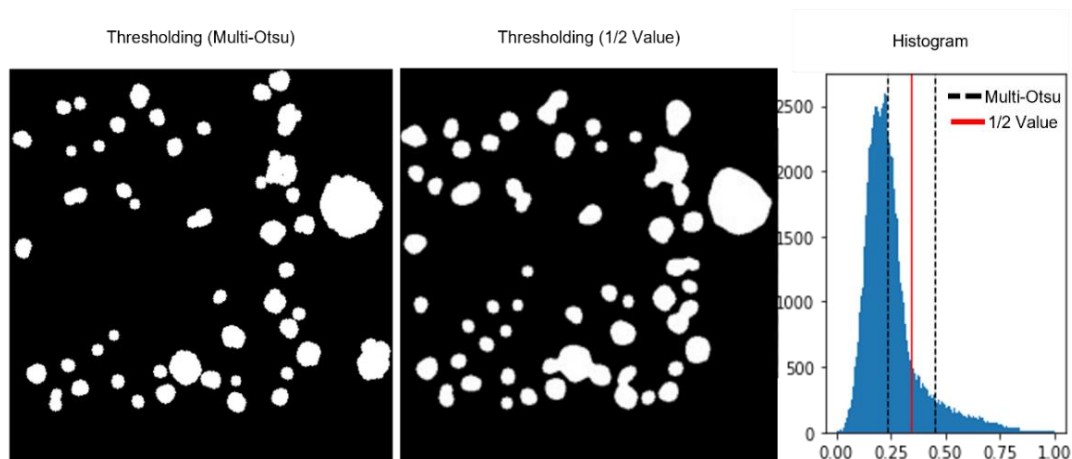


### II. Filtering

The noise level of the image from the liquid cell was too high to be processed directly. To reduce noise efficiently, several filtering techniques (Gaussian filter, Bilateral filter, and Erosion & Dilation) were applied.

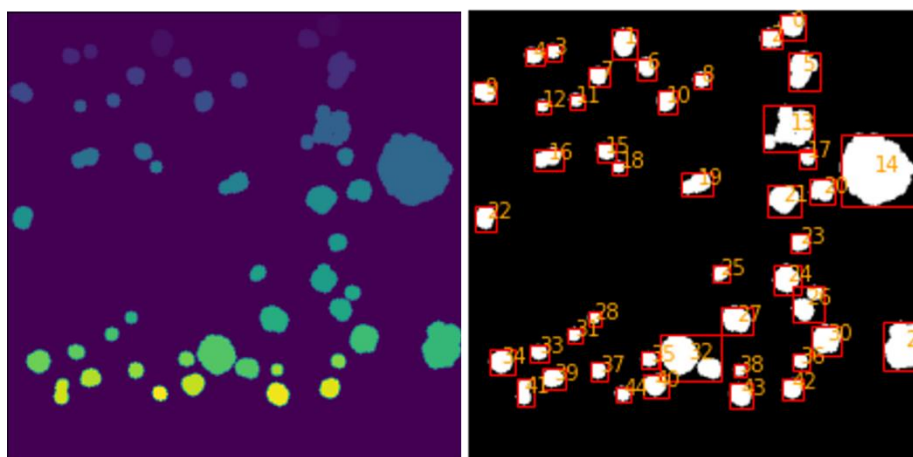
### III. Thresholding

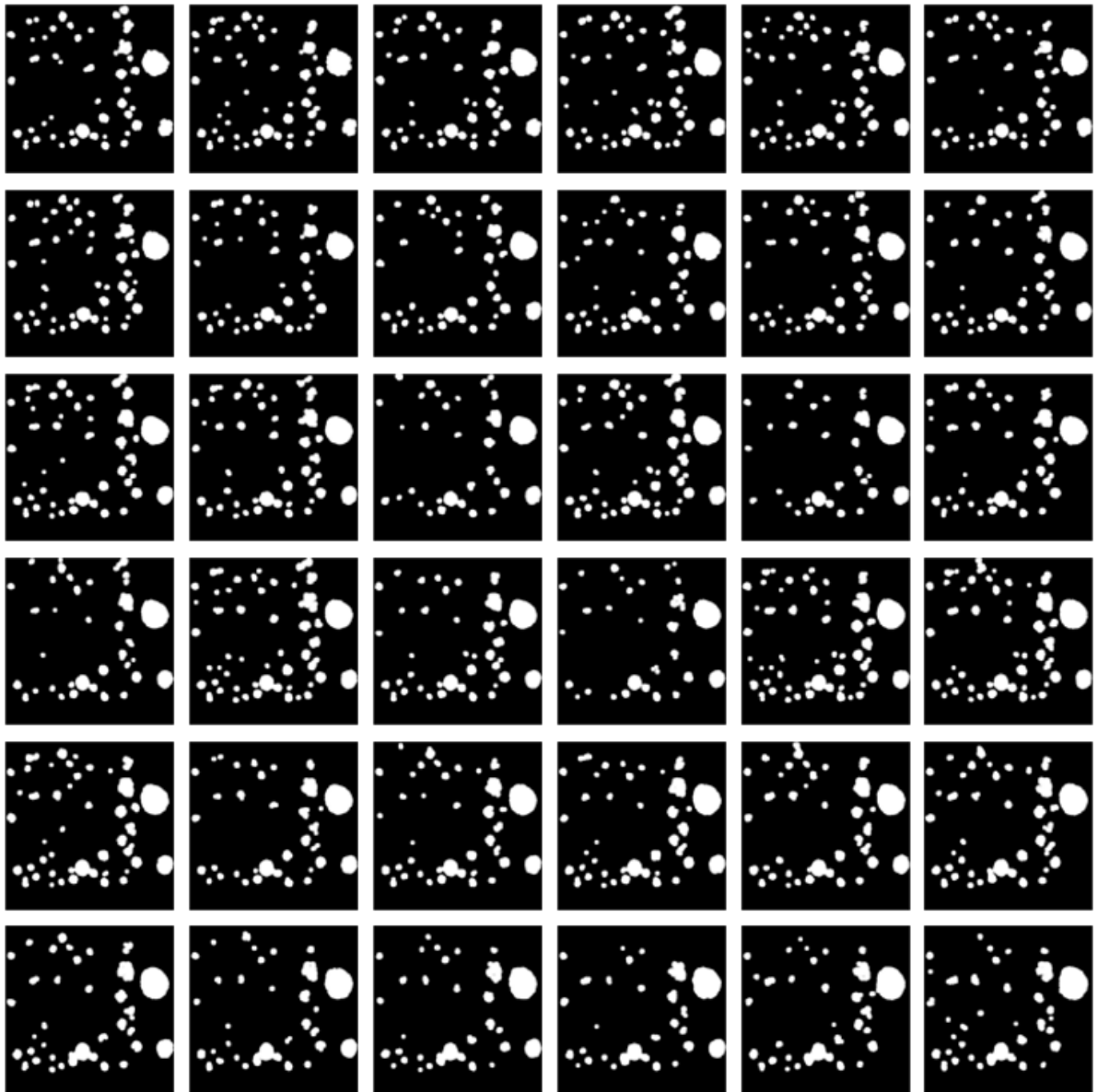
Multi-Otsu is a well-known algorithm to find optimal values to create binary images. In this paper, the mean value of the multi-Otsu result (red) was selected for thresholding for estimating the number of particles and size distribution. Whereas the lower multi-Otsu value (right dotted line) was used to calculate the particle growth rates. Based on the selected value, each pixel becomes 0 (lower, black, background) or 1 (higher, white, target) by thresholding. After thresholding, the white region attached to the image border was removed to avoid wrong statistics.



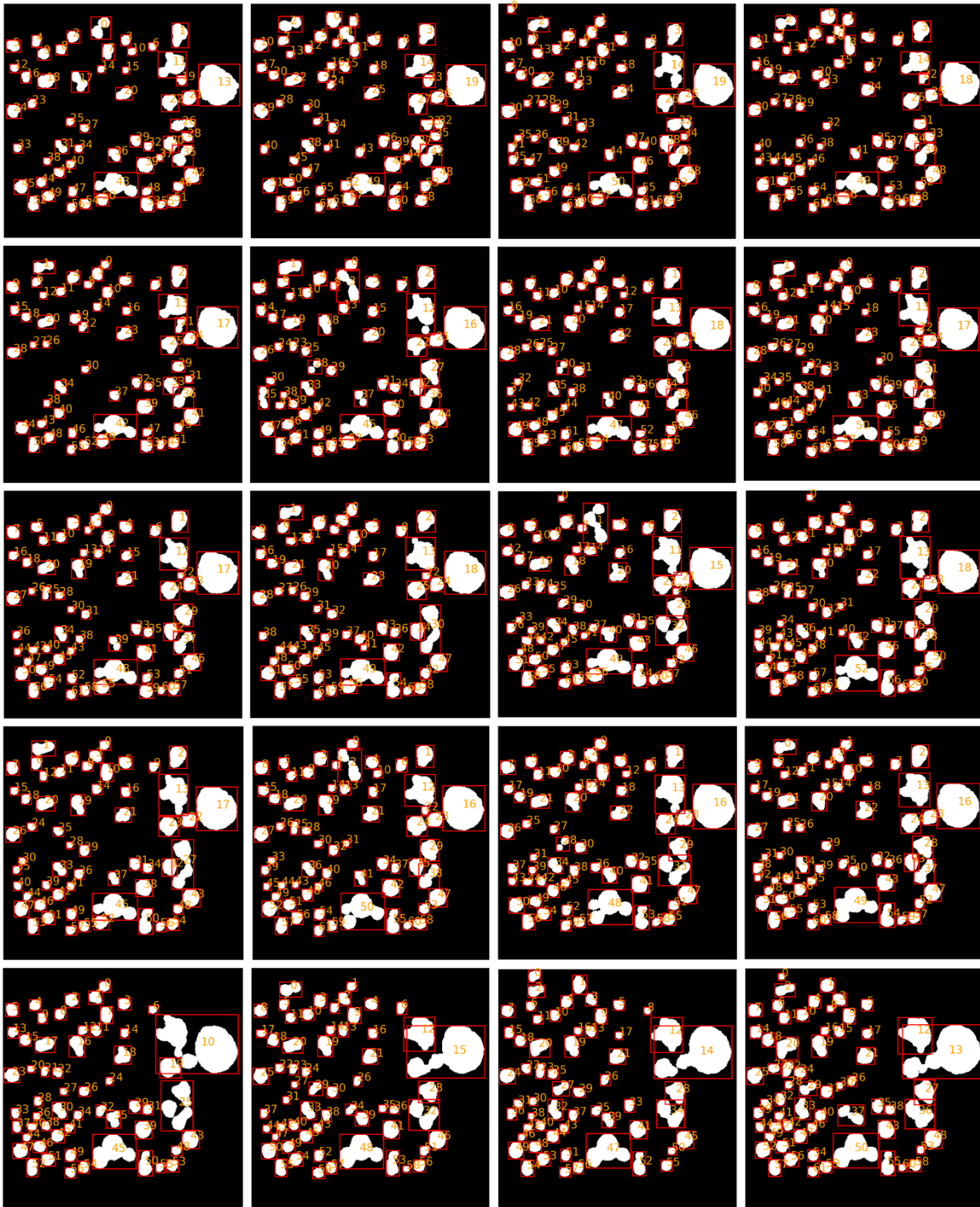
### IV. Segmentation

After thresholding, each white region can be recognised as a single particle. The number of particles was the same as the number of white regions. As the shape of the particles was assumed to be a circle, the diameter of each particle was calculated from the area of each white region with pixel-to-nanometer calibration. Based on position, the diameter of the particle was tracked through the video series.





**Supplementary Fig. 23:** Every third frame of a video series containing 114 frames after thresholding (multi-Otsu). The growth rates of particles in Fig. 3c were estimated using these images. (1<sup>st</sup> image is the initial frame and the last image is the 109<sup>th</sup> frame)



**Supplementary Fig. 24:** Every sixth frame of a video series containing 114 frames after thresholding (1/2 value). The number of particles formed with time during the anti-solvent crystallisation (Fig. 3b) was estimated using such images from all the frames. (1<sup>st</sup> image is the initial frame and the last image is the 114<sup>th</sup> frame.)

## 6 Supplementary Tables

**Supplementary Table 1: Values of *d*-spacings obtained from powder XRD patterns of R-BINOL-CN.**

<b>2<math>\theta</math></b>	10	12.5	13.5	15.5	17.2	18.7	20	21.7	24	25.7	27.8	31.4	32.2
<b><i>d</i> (Å)</b>	8.83	7.07	6.55	5.71	5.15	4.74	4.43	4.09	3.70	3.46	3.20	2.85	2.78

## 7 List of Movies and Captions

**Supplementary Movie 1:** Animation illustrating the liquid mixing procedure employed to perform anti-solvent crystallisation using the DENSsolution liquid cell holder. A summary of all other experiments is presented. The tip configuration shown is for a JEOL microscope-compatible holder.

**Supplementary Movie 2:** STEM-ADF movie showing precipitation of particles in real-time via anti-solvent crystallisation. A solution of R-BINOL-CN dissolved in chloroform is initially present in the viewing area to which methanol is mixed. The time interval between each frame is 2.16 s. (10 fps) (DENSsolutions Stream)

**Supplementary Movie 3:** BF-TEM movie showing the bottom chip after the end of the in-situ mixing experiment. The liquid cell was disassembled and only the bottom chip is fixed on the holder.

**Supplementary Movie 4:** STEM-ADF movie showing growth of an R-BINOL-CN particles growing on different silicon nitride windows during the anti-solvent crystallisation process. The time interval between each frame is 2.16 s. (10 fps) (DENSsolutions Stream)

**Supplementary Movie 5:** STEM-ADF movie showing particle growth by monomer addition and coalescence in a solution of R-BINOL-CN dissolved in chloroform. The time interval between each frame is 2.16 s. (10 fps) (DENSsolutions Stream)

**Supplementary Movie 6:** STEM-ADF movie showing Ostwald Ripening in a solution of R-BINOL-CN dissolved in chloroform. The time interval between each frame is 2.16 s. (10 fps) (DENSsolutions Stream)

**Supplementary Movie 7:** STEM-ADF movie showing growth of R-BINOL-CN nanoparticles via oriented attachment (OA). The time interval between each frame is 2.16 s. (10 fps) (DENSsolutions Stream)

**Supplementary Movie 8:** Animation of the holder tip showing the configuration of the two chips and O-rings which form the liquid cell assembly. (Thermo Fischer Scientific compatible holder)

**Supplementary Movie 9:** Animation of the chip assembly showing the flow channel on the bottom chip. (Thermo Fischer Scientific compatible holder)

**Supplementary Movie 10:** Animation of a liquid entering the Nano-Cell and flowing across the on-chip microfluidic channel defined by the spacers. (Thermo Fischer Scientific compatible holder)

**Supplementary Movie 11:** TEM movie showing quick entry of liquid into the viewing of the liquid cell. The change in contrast observed across the viewing area indicates the fluid entry. (DENSsolutions Stream)

**Supplementary Movie 12:** TEM movie showing quick entry of liquid into the viewing of the liquid cell. (DENSsolutions Stream)

**Supplementary Movie 13:** STEM-ADF movie showing poor contrast due to large liquid layer thickness. We try to follow the growth kinetics using a solution of R-BINOL-CN dissolved in chloroform. The time interval between frames is 3 s. (4 fps) (DENSsolutions Ocean)

**Supplementary Movie 14:** STEM-ADF movie showing particle growth in a solution of R-BINOL-CN dissolved in chloroform. A reasonably good contrast was achieved after several attempts. The time interval between frames is 3 s. (10 fps) (DENSsolutions Ocean)

**Supplementary Movie 15:** STEM-ADF movie of particle growth trials in a solution of R-BINOL-CN dissolved in chloroform. The time interval between frames is 3 s. (10 fps) (DENSsolutions Stream Holder)

## 8 Supplementary References

20. Ianiro, A. *et al.* Liquid–liquid phase separation during amphiphilic self-assembly. *Nat Chem* **11**, 320–328 (2019).
22. Rizvi, A., Mulvey, J. T. & Patterson, J. P. Observation of Liquid–Liquid-Phase Separation and Vesicle Spreading during Supported Bilayer Formation via Liquid-Phase Transmission Electron Microscopy. *Nano Lett* **21**, 10325–10332 (2021).
31. van Omme, J. T. *et al.* Liquid phase transmission electron microscopy with flow and temperature control. *J Mater Chem C Mater* **8**, 10781–10790 (2020).
53. van Deursen, P. M. G. *et al.* Graphene Liquid Cells Assembled through Loop-Assisted Transfer Method and Located with Correlated Light-Electron Microscopy. *Adv Funct Mater* **30**, (2020).
54. Cookman, J., Hamilton, V., Price, L. S., Hall, S. R. & Bangert, U. Visualising early-stage liquid phase organic crystal growth: Via liquid cell electron microscopy. *Nanoscale* **12**, 4636–4644 (2020).
55. Rasband, W.S., ImageJ, U.S. National Institutes of Health, Bethesda, Maryland, USA, <https://imagej.nih.gov/ij/>, 1997-2018.
56. Schneider, C.A., Rasband, W.S., Eliceiri, K.W. "NIH Image to ImageJ: 25 years of image analysis". *Nature Methods* **9**, 671-675, 2012.
57. Abramoff, M.D., Magalhaes, P.J., Ram, S.J. "Image Processing with ImageJ". *Biophotonics International*, volume **11**, issue 7, pp. 36-42, 2004.
58. Wieting, J.M., Fisher, T.J., Schafer, A.G., Visco, M.D., Gallucci, J.C., Mattson, A.C. Preparation and Catalytic Activity of BINOL-Derived Silanediols. *Eur. J. Org. Chem.* **2015**, 525-533 (2015).